Supplemental Material

Selective inhibition of CDK7 reveals high-confidence targets and new models for TFIIH function in transcription

Rimel, JK[1§]; Poss, ZC[2§]; Erickson, B[3,4]; Maas, ZL[1,2,5]; Ebmeier, CC[2]; Johnson, JL[6]; Decker, T-M[1]; Yaron, TM[6,7]; Bradley, MJ[8]; Hamman, KB[8]; Hu, S[8]; Malojcic, G[8]; Marineau, JJ[8]; White, PW[9]; Brault, M[9]; Tao, L[9]; DeRoy, P[9]; Clavette, C[9]; Nayak, S[10]; Damon, LJ[1,5]; Kaltheuner, IH[11]; Bunch, H[12]; Cantley, LC[6]; Geyer, M[11]; Iwasa, J[10]; Dowell, RD[2,5]; Bentley, DL[3,4]; Old, WM[2*]; Taatjes, DJ[1,13*]

[1] Dept. of Biochemistry, University of Colorado, Boulder, CO 80303, USA.
[2] Dept. of Molecular, Cellular, and Developmental Biology, University of Colorado, Boulder, CO 80309, USA.
[3] Dept. Biochemistry and Molecular Genetics, University of Colorado School of Medicine, Aurora, CO 80045, USA.
[4] UC-Denver RNA Bioscience Initiative
[5] BioFrontiers Institute, University of Colorado, Boulder, CO 80309, USA.
[6] Meyer Cancer Center, Weill Cornell Medicine, New York, NY, 10065, USA.
[7] Englander Institute for Precision Medicine, Institute for Computational Biomedicine, Department of Physiology and Biophysics, Weill Cornell Medicine, New York, NY 10065, USA.
[8] Syros Pharmaceuticals, 35 CambridgePark Drive, 4th floor Cambridge, MA 02140 USA.
[9] Paraza Pharma, Inc., 2525 Marie Curie Montreal, QC Canada.
[10] Dept. of Biochemistry, University of Utah, Salt Lake City, UT, USA.
[11] Institute of Structural Biology, University of Bonn, Germany.
[12] School of Applied Biosciences, College of Agriculture and Life Sciences, Kyungpook National University, Republic of Korea.
[13] Lead contact
§equal contribution
**corresponding authors*

Supplemental Fig_1

A

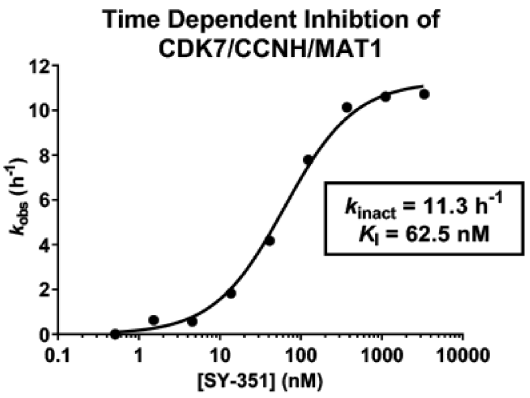

B

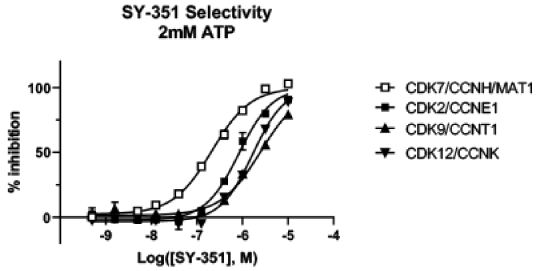

Supplemental Figure 1. Additional details about SY-351.
(A) SY-351 is a potent and time-dependent inhibitor of active CDK7/CCNH/MAT1 with a k_{inact} of 11.3 h^{-1} and K_I of 62.5 nM.
(B) SY-351 inhibition of active kinases CDK7/CCNH/MAT1, CDK2/CCNE1, CDK9/CCNT1, CDK12/CCNK with 2mM ATP. The best fit IC_{50} values are 205 nM, 988 nM, 2237 nM, and 1554 nM, respectively.

Supplemental Fig_S2

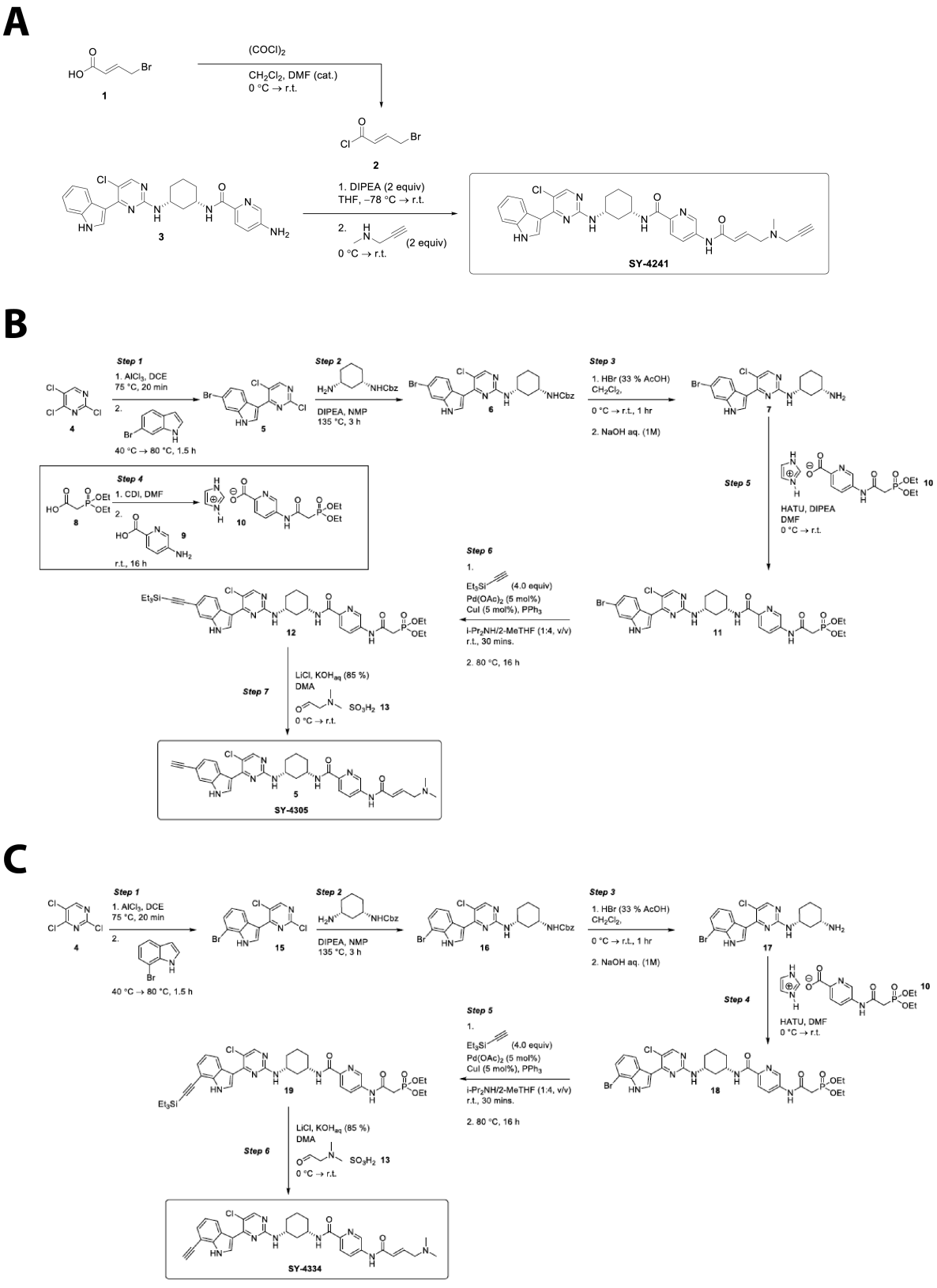

Supplemental Figure 2. Chemical structures and synthesis of alkyne probes used in ABPP experiments.

(A) Overview for SY-4241, (B) SY-4305, and (C) SY-4334.

Supplemental Fig_3

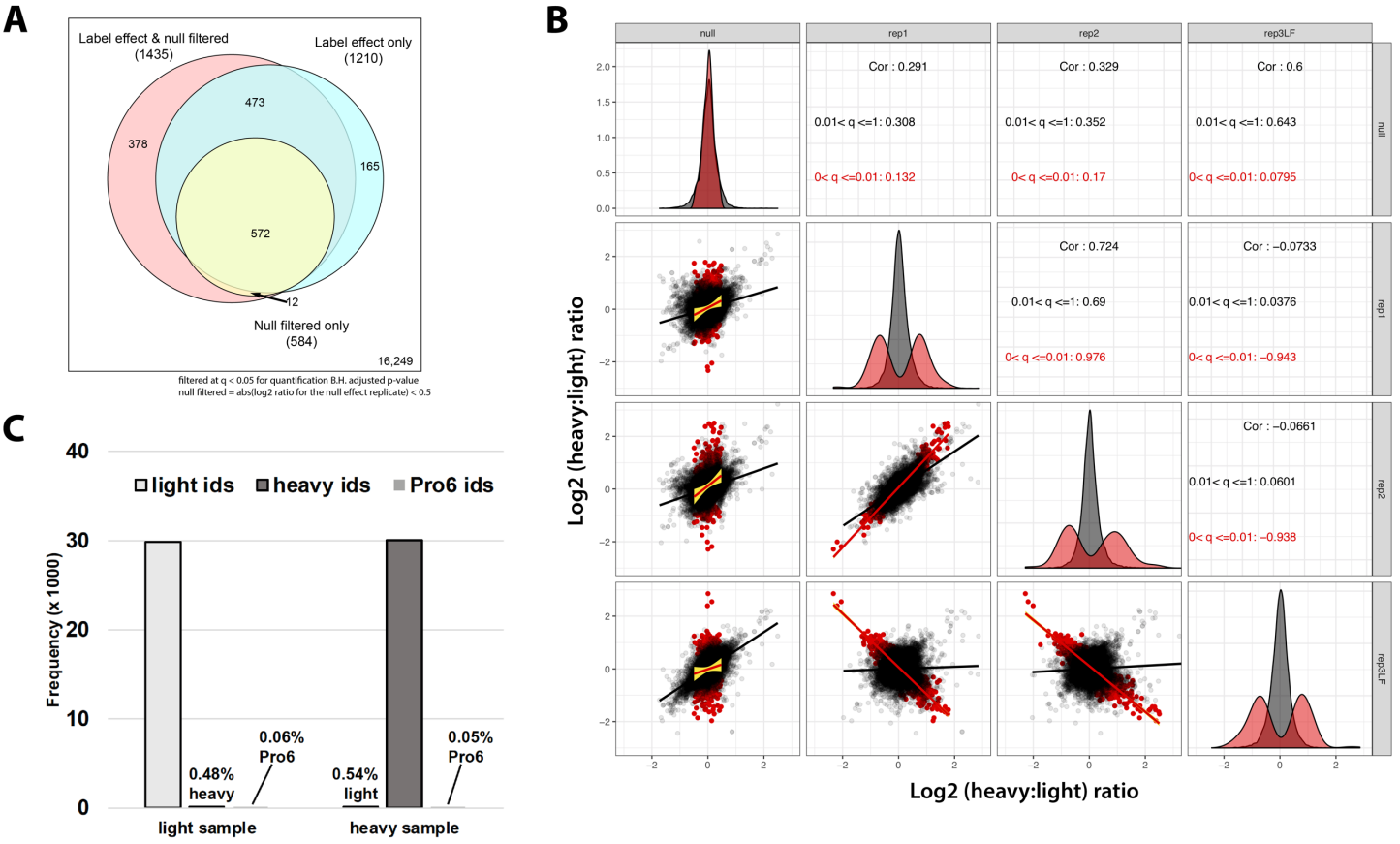

Supplemental Figure 3. Improved modeling of SY-351 treatment effect with a two-parameter linear model.
(A) Two different linear models were tested, coded in R and based on the limma package (Ritchie et al. 2015). The "Label effect" (isotope effect) model incorporates an extra coefficient in addition to the drug effect coefficient to explicitly model systematic bias in the SILAC isotope ratios present prior to drug treatment. This provides improved modeling of the residual errors, and as a result, improved detection of significant phosphorylation sites changing with SY-351. In addition, we evaluated the effect of removing SILAC ratios showing large changes (| log2(Heavy/Light) | > 0.5) "null filtered" in combination with the two coefficient model "Label effect & null filtered" vs. "Label effect only". "Null filtered only" is the simple model with only one coefficient for the SY-351 effect with large magnitude log2 ratios in the null condition removed prior to testing.
(B) The label (a.k.a. isotope) effect captured by the coefficient β_{g0}, and the SY-351 specific effect captured by the coefficient β_{g1}, can be seen in scatterplots of the $\log_2$ (heavy/light) ratios**,** as on-diagonal grey points, and red points, respectively, superimposed on scatterplots for each sample**.** The effect of the isotope-label flip comparison for differentially expressed phospho-sites can be seen as the negative correlation of red points when compared with the non-swapped conditions. The isotope bias effect can be seen as a non-zero correlations in the comparisons with the null condition (first column of scatterplots), and the superposition of these correlated sites in the flipped sample (rep3LF) comparisons. The on-diagonal panels show the $\log_2$ (heavy/light) ratio distributions for phospho-site SILAC ratios found to be differentially expressed with SY-351 at $q \leq 0.01$ (red) and those that did not reach this threshold at $q > 0.01$ (grey). For each of the six sample comparison scatterplots in the lower left of the matrix, the significant (red) and non-significant (grey) phospho-site $\log_2$ (heavy/light) ratios are plotted, and a smoothed linear fit to the points in each group (red and grey) is plotted to highlight the degree and direction of correlation. The Pearson correlation coefficients for each scatterplot are shown in the panels in the upper triangle, showing both the overall correlation (top of each panel) and the correlation for each group separately.
(C) Metabolic incorporation analysis of searches from heavy- and light-labeled HL-60 samples. In both samples, heavy and light modifications (see Methods) were searched, as well as Arg-->Pro conversion. Data were analyzed from the evidence file and showed low levels of unmodified peptides in the sample of interest, suggesting isotopic incorporation into cellular proteomes was essentially complete, and proline conversion very low.

Supplemental Fig_4

A

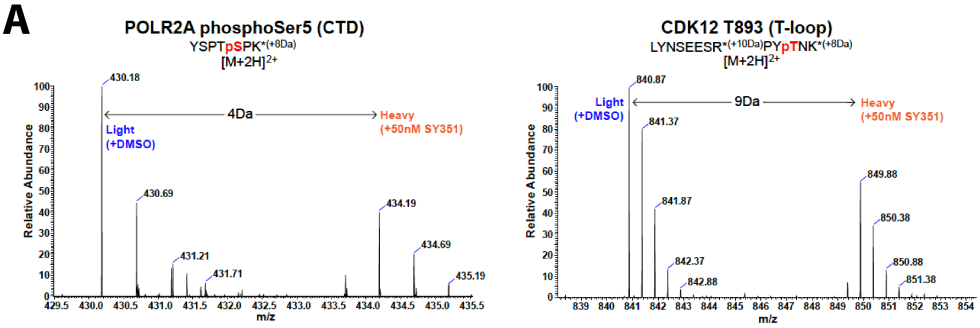

B

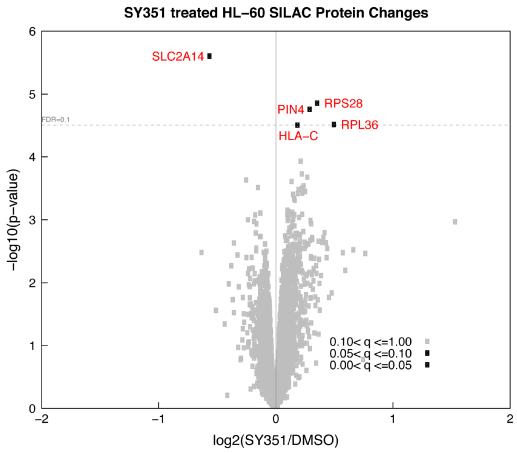

C

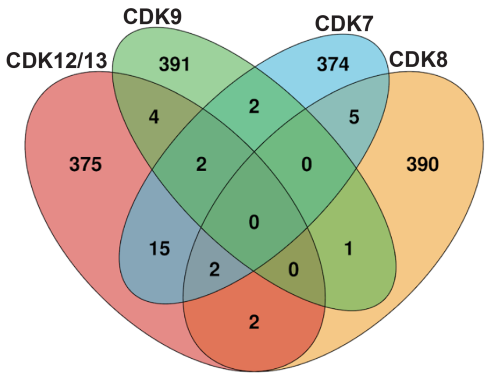

shared kinase targets

Splicing	RNA processing
SF3B1	DDX21
CASC3	MATR3
DGCR14	MEPCE
RBM25	
THRAP3	**Cell Cycle**
	CDC5L
Transcription	
FOXK1	**Other**
GATAD2B	AGFG1
SUPT5H	SEC22B

D

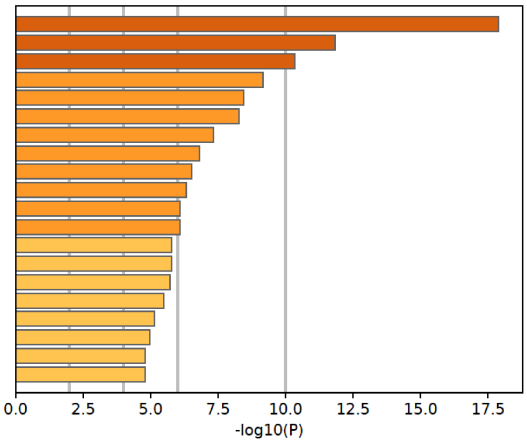

GO:0006397: mRNA processing
GO:0050657: nucleic acid transport
GO:0000018: regulation of DNA recombination
GO:0080135: regulation of cellular response to stress
GO:0033044: regulation of chromosome organization
GO:1903311: regulation of mRNA metabolic process
R-HSA-69278: Cell Cycle, Mitotic
R-HSA-194315: Signaling by Rho GTPases
GO:0007017: microtubule-based process
GO:0010638: positive regulation of organelle organization
R-HSA-75153: Apoptotic execution phase
GO:0051301: cell division
GO:0006354: DNA-templated transcription, elongation
GO:0051347: positive regulation of transferase activity
GO:1903312: negative regulation of mRNA metabolic process
GO:0043547: positive regulation of GTPase activity
GO:0045727: positive regulation of translation
GO:0097190: apoptotic signaling pathway
GO:0046831: regulation of RNA export from nucleus
GO:0010639: negative regulation of organelle organization

Supplemental Figure 4. Few proteins change in abundance with SY-351 treatment; summary of phosphoproteins with significantly decreasing phospho-sites.

(A) MS scans of key SILAC pairs identified in this study. The Ser5 repeat POLR2A is a recognized CDK7 substrate, and was identified upon inhibition with SY-351 treatment. The 4Da difference is reflected in the 8Da mass difference in the peptide pair, and accounted for by the +2 charge. T893 of CDK12 is a regulatory "T-loop" phosphorylation site, and the 9Da difference is reflected by the 18Da peptide difference, as there is a missed cleavage due to a C-terminal proline adjacent to an internal arginine, and accounted for by the +2 charge. Note that for both peptide pairs, the heavy sample was treated with SY-351, accounting for the reduced abundance of the heavy phosphopeptide. Also note that the ratiometric abundance of these peptide pairs was not recapitulated in the null sample, without SY-351 treatment, and that the Ser2 POLR2A peptide, which is not a generally recognized CDK7 substrate, did not show this decrease with SY-351 treatment (not shown).

(B) In parallel to the phosphoproteome experiment, we also performed SILAC proteomics to test whether SY-351 treatment led to protein-level changes. Statistical analysis for protein-level SILAC ratios was identical to the phosphoproteome analysis using the same two-coefficient modeling approach.

(C) Venn diagram showing phosphorylation sites shared or mutually exclusive for transcription-associated kinases CDK7, CDK8, CDK9, and CDK12/CDK13. For each kinase, the top 400 identified phosphorylated proteins, based upon the largest negative log-fold change values and $p < 0.05$, were used for comparisons, and the number of overlapping proteins was calculated for all combinations of samples. CDK7 targets identified here were compared with proteins identified as substrates for CDK8 in HCT116 cells (Poss et al. 2016), CDK9 in HCT116 cell extracts (Sanso et al. 2016), and CDK12/13 in IMR-32 and Kelly cells (Krajewska et al. 2019).

(D) Metascape GO and pathway analysis of phosphosites whose ratios decreased with SY-351 treatment ($q<0.05$). This analysis shows the top 20 enriched GO terms and pathways (see Methods). Note that the top enriched GO term is mRNA processing, and that multiple terms associated with RNA processing are present. For increased phosphosites, terms associated with mRNA processing were also enriched (not shown). "R-HSA" refers to Reactome pathway nomenclature.

Supplemental Fig_5

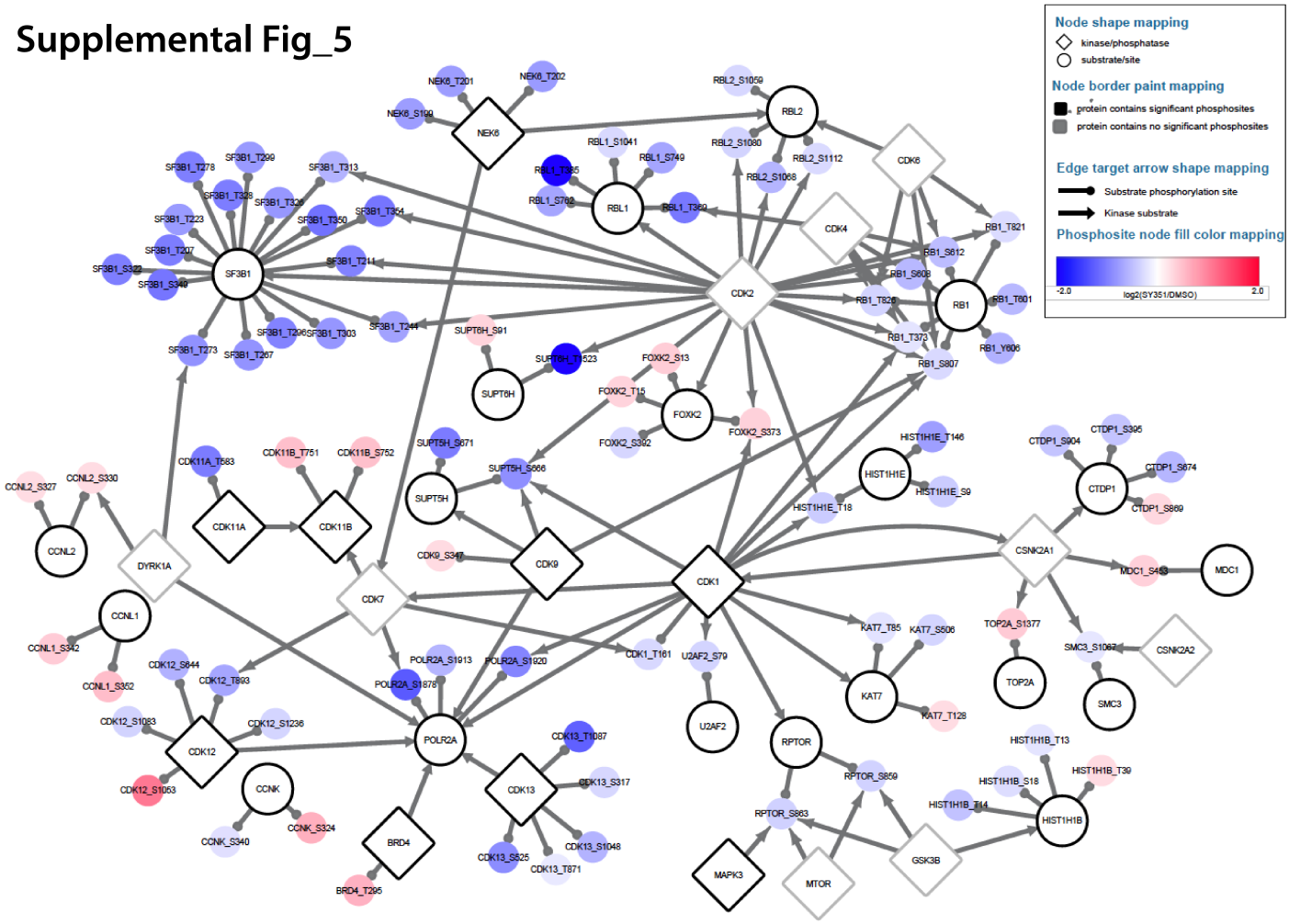

Supplemental Figure 5. Kinase-substrate network of SY-351 responsive phosphorylation sites. Phosphorylation sites that changed significantly after 1 hour treatment of HL-60 cells with 50 nM SY-351 (CDK7 inhibitor) are shown, as well as known kinases for those sites, some of which were not observed with significantly changing phospho-sites, e.g. CDK7. The network shown is a subnetwork manually selected from the larger parent network to emphasize only the kinases and substrates within a few degrees of separation from CDK7, CDK9, and POLR2A. Phosphorylation sites were filtered at q-value < 0.05, and overlaid onto a kinase substrate network using Cytoscape. Color is mapped to the log2 (SY-351/DMSO) ratio.

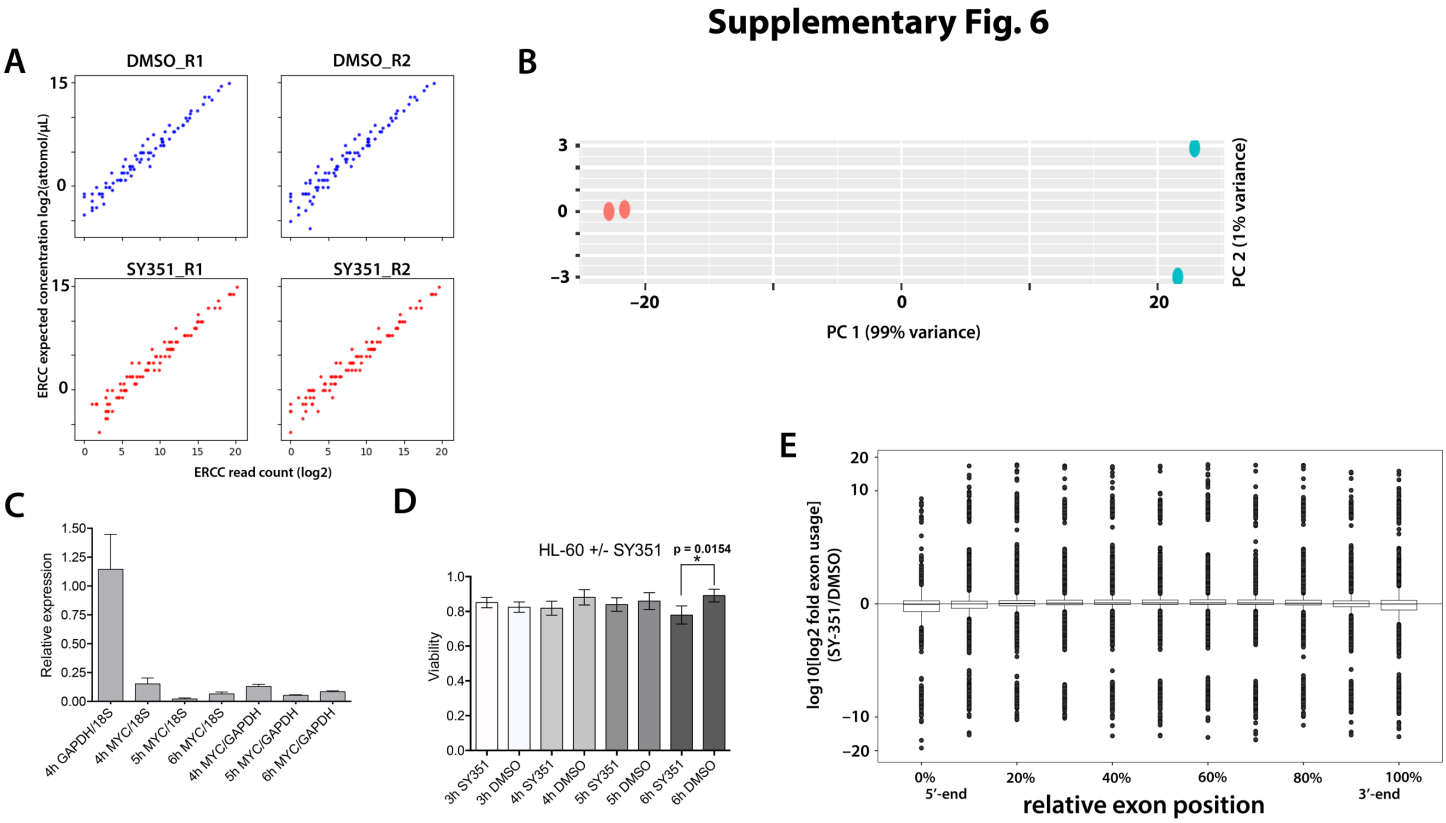

Supplemental Figure 6. Additional information about RNA-seq experiments in HL60 cells.
(A) ERCC spike-in normalization.
(B) PCA plot for RNA-seq replicates.
(C) RNA levels, measured at t = 5h (RT-qPCR) after treatment of HL60 cells with 50 nM SY-351 (vs. DMSO controls). Expression of MYC was markedly reduced upon CDK7 inhibition, as expected (Kwiatkowski et al. 2014).
(D) Time course of HL60 cell viability following 50 nM SY-351 treatment.
(E) Summary of DEXSeq analysis of genes with more than 10 exons (n = 9767), that compared SY-351 vs. control DMSO cells. Results indicate no loss of exon usage toward gene 3'-ends with SY-351 treatment, which suggests that "off-target" CDK12 inhibition is not occurring. With CDK12 inhibition or knockdown, intronic polyadenylation occurs, causing reduced exon usage toward gene 3'-ends (Dubbury et al. 2018; Krajewska et al. 2019). Note that the box plots were generated after normalizing the log2-fold change data using the pseudo-log10 transformation (asinh(x/2)/log(10)).

Supplemental Fig_7

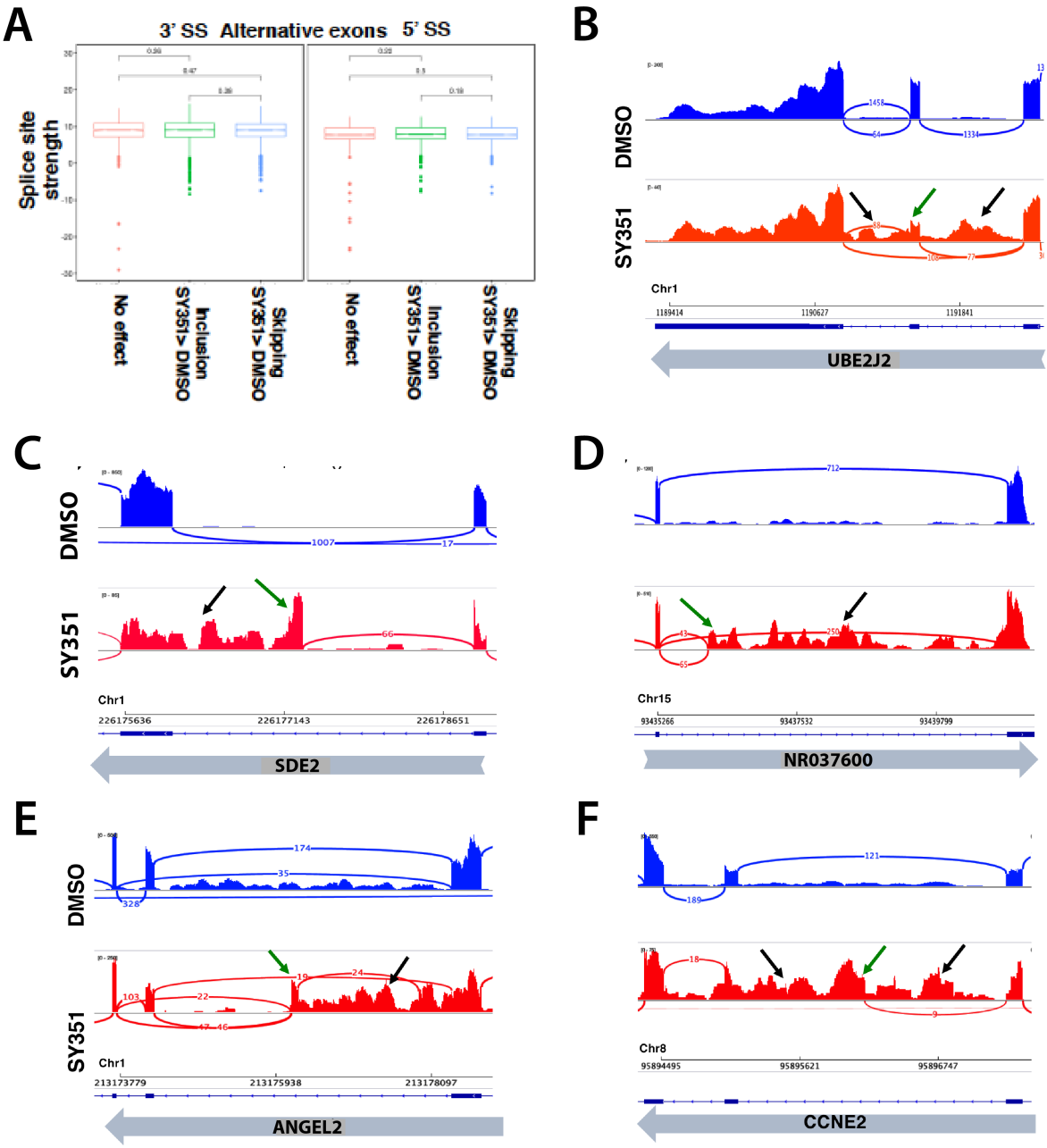

Supplemental Figure 7. Alternative splicing events affected by SY-351.
(A) Alternative spliced exons affected by SY-351 do not have significantly different 5' or 3' splice site strength from unaffected alternative splicing events. Splice site strengths were calculated according to (Yeo et al. 2004).
(B-F) IGV genome browser Sashimi plots of differential exon inclusion with associated reduction in splicing of flanking introns. Normalized read numbers for DMSO control and SY-351 treated samples are shown on the Y axis. Splice junction read numbers for sense strand transcripts are shown in blue and red. Screen shots are shown for individual RNA-seq data sets. In all cases the changes caused by SY-351 were reproduced in a biological replicate. Green arrows denote changes in exon inclusion; black arrows denote changes in intron retention.

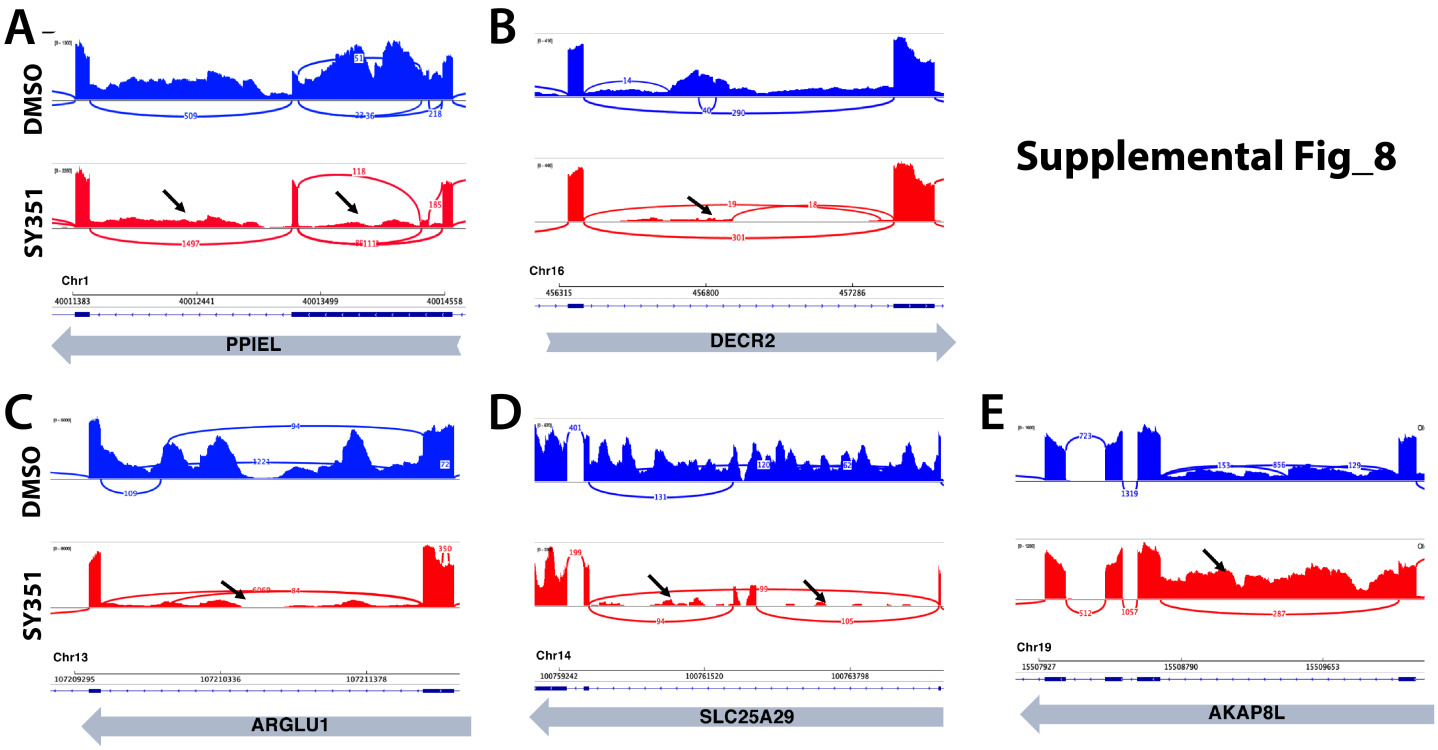

Supplemental Figure 8. Alternative intron retention affected by SY-351.
(A-D) IGV genome browser Sashimi shots showing increased splicing of retained introns (black arrows) in SY-351.
(E) Decreased splicing of a retained intron (black arrow) in SY-351.

Supplementary Fig. 9

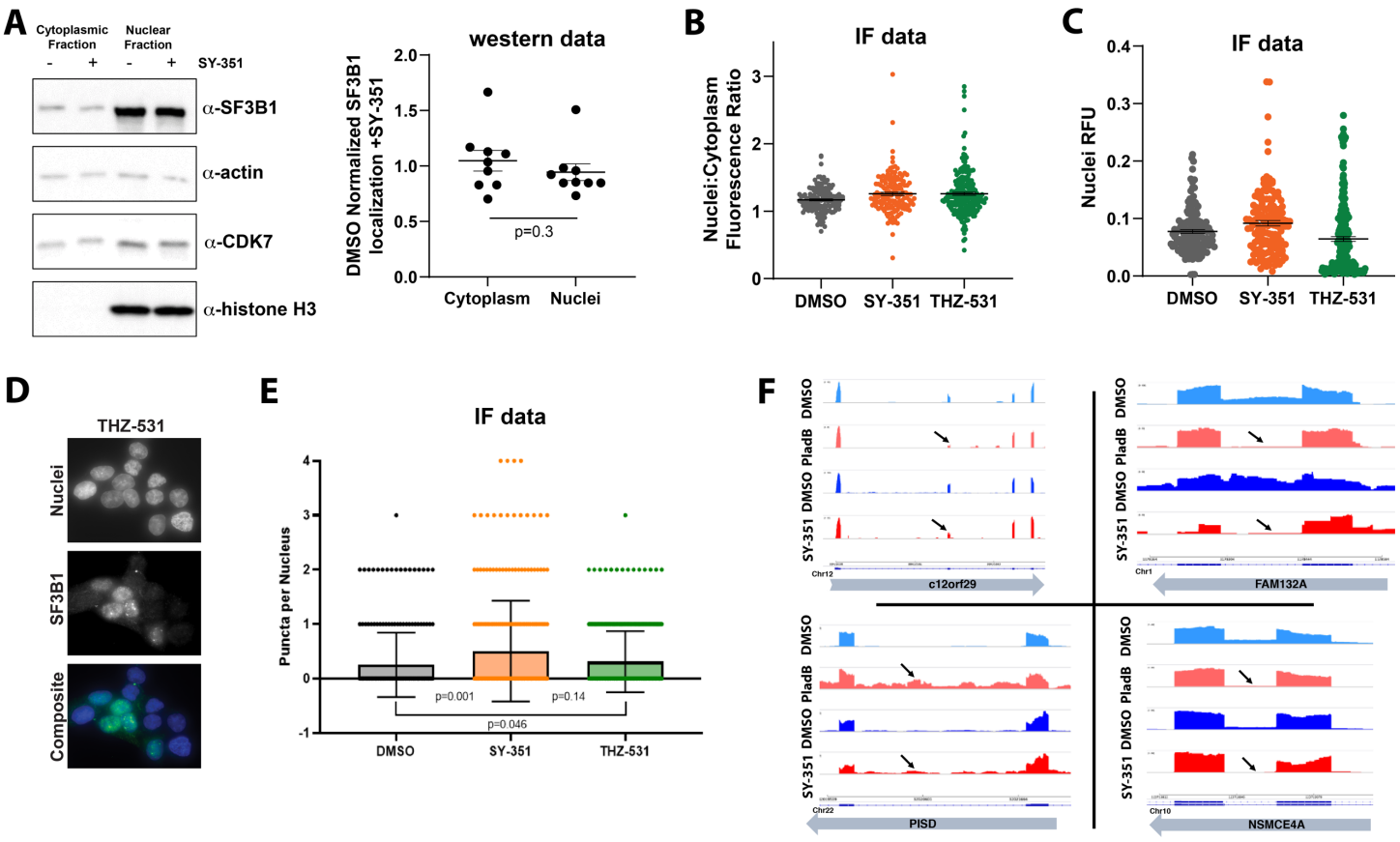

Supplemental Figure 9. SY-351 alters SF3B1 localization to nuclear speckles.
(A) Quantitative westerns across replicates evaluating endogenous SF3B1 localization to the cytoplasm vs. nucleus, +SY-351 conditions normalized to DMSO (biological, n=3; technical, n=3).
(B) SF3B1 immunofluorescence data illustrating no significant difference in SF3B1 localization in treatment conditions, p>0.9.
(C) SF3B1 IF further indicating no significant change in overall nuclear relative fluorescence in DMSO vs. treatment conditions (SY-351 p=0.3 and THZ-531 p=1.0 relative to DMSO, SY-351 p=0.1 relative to THZ-531).
(D) Immunofluorescence microscopy of endogenous SF3B1 (green) and Hoescht (blue) in THZ-531 conditions.
(E) Quantitation of SF3B1 puncta per nucleus in DMSO vs. SY-351 vs. THZ-531 conditions (n=3 biological replicates).
(F) Representative traces of genes that exhibit similar splicing defects in SY-351 (CDK7 inhibition) and PladB-treated cells (SF3B1 inhibition), respectively.

Supplementary Fig. 10

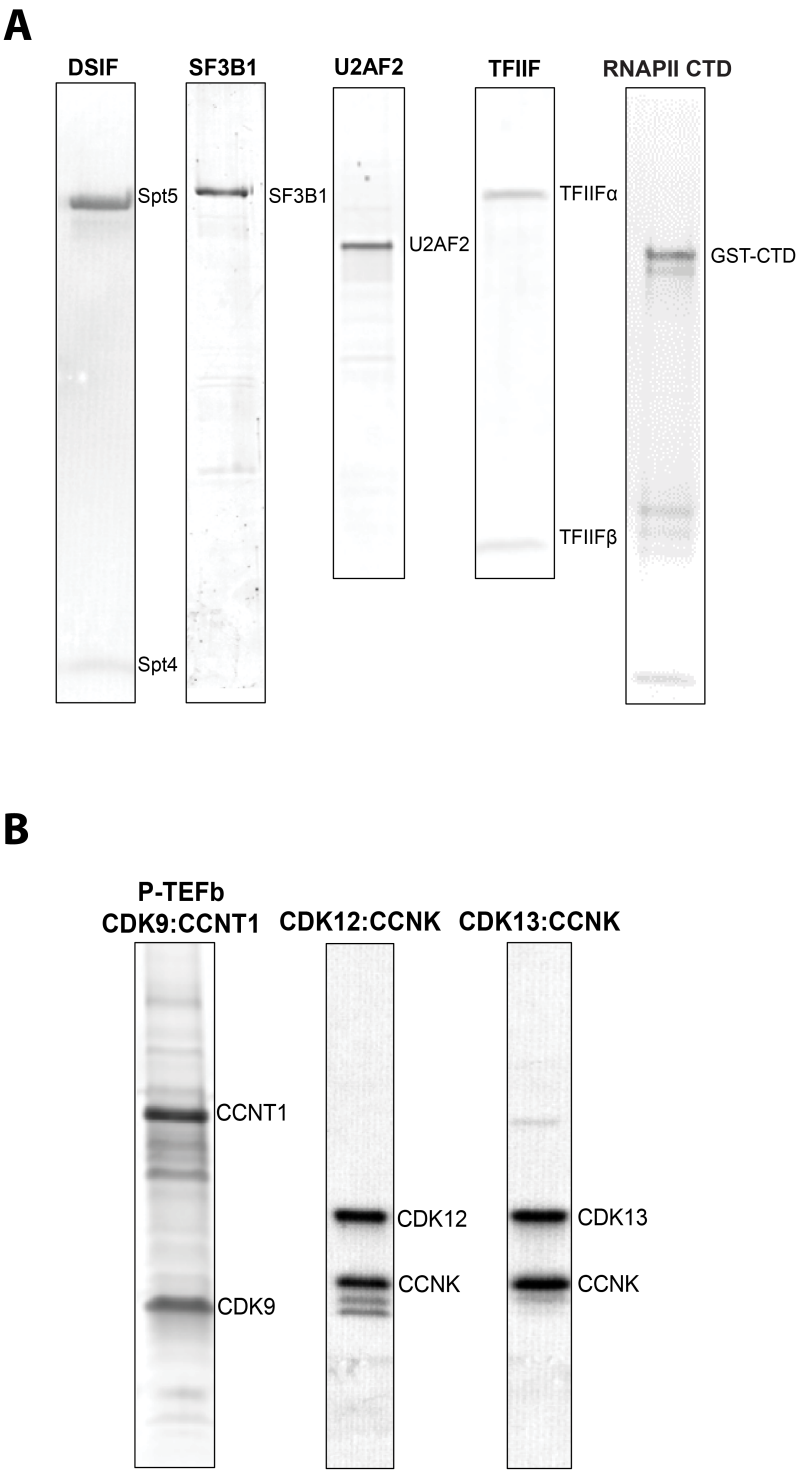

Supplemental Figure 10. Purified factors used for *in vitro* kinase assays.
(A) Kinase substrates.
(B) Kinase complexes.

Supplementary Fig. 11

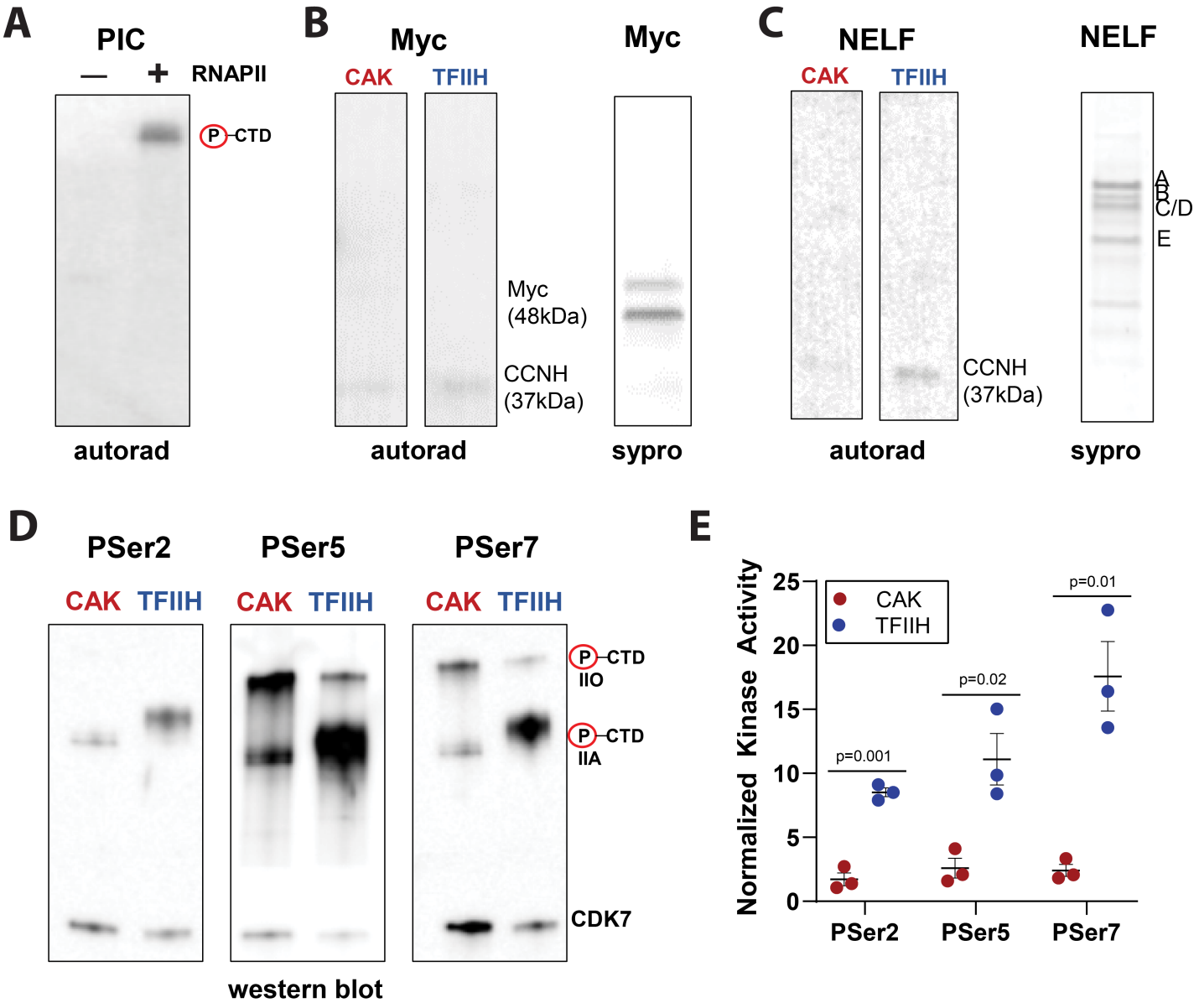

Supplemental Figure 11. Additional *in vitro* kinase results.
(A) TFIIH phosphorylation of the RNAPII CTD in a transcriptionally active promoter-assembled PIC. The PIC was assembled at the HSPA1B promoter as described (Fant et al. 2020) and contained TFIIA, TFIIB, TFIID, TFIIE, TFIIF, TFIIH, and Mediator. RNAPII was excluded (–) or added as indicated.
(B, C) CDK7 does not directly phosphorylate MYC (A) or NELF (B) *in vitro*.
(D) Analysis of RNAPII CTD Ser2-, Ser5- and Ser7-phosphorylation by western blot, comparing CDK7 activity within the CAK or TFIIH.
(E) Quantitation of data from panel D, across biological replicates (n=3) with western signal normalized to CDK7

Supplementary Fig. 12

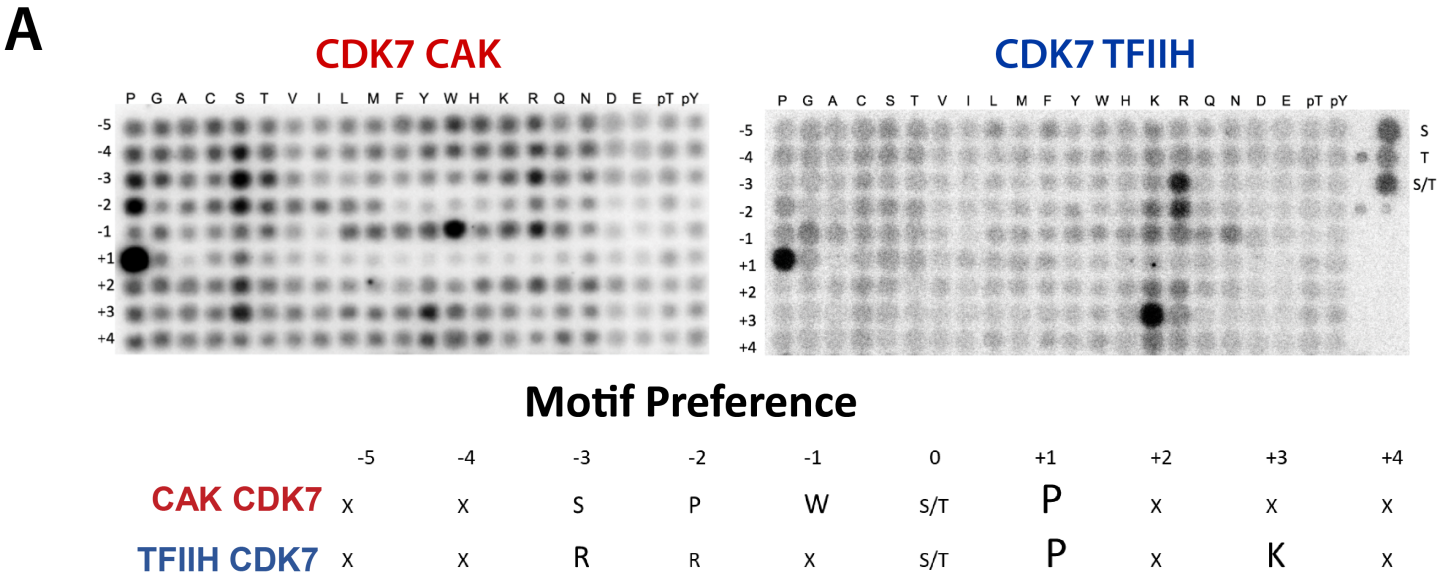

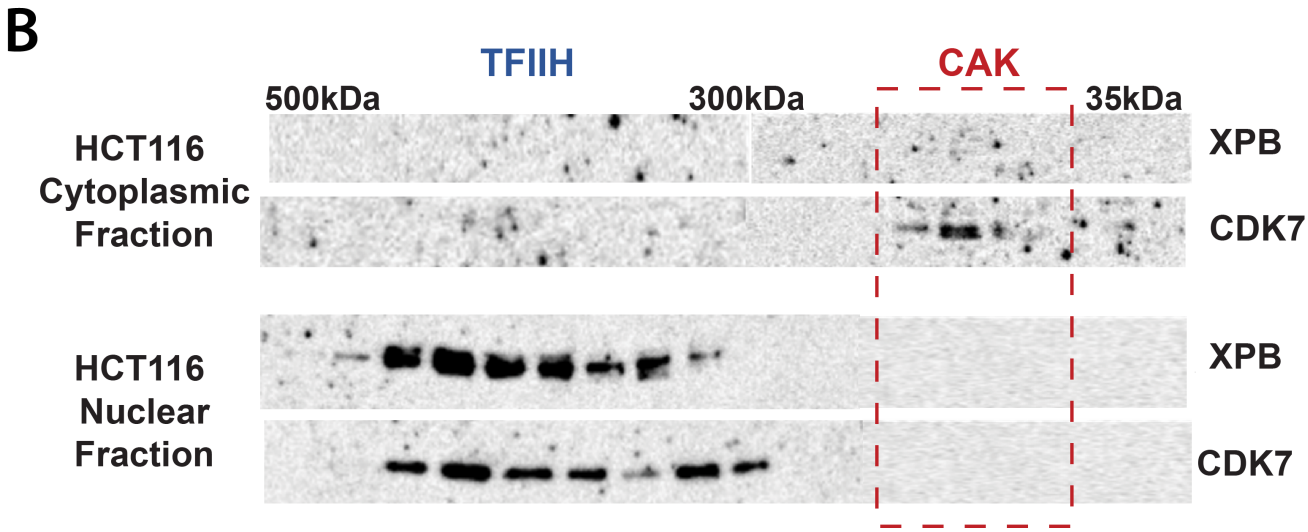

Supplemental Figure 12. CAK and TFIIH motif preference and cellular localization
(A) Peptide array experiments (Begley et al. 2015) indicate distinct substrate preferences for CDK7 as part of TFIIH or the CAK.
(B) CDK7 does not appear to be present in CAK complexes in the nucleus. Western blots were performed across fractions from a size-exclusion column. Cytoplasmic vs. nuclear fractions were probed; as expected, the CAK was detected in the cytoplasm and TFIIH was detected in the nucleus.

Supplementary Fig. 13

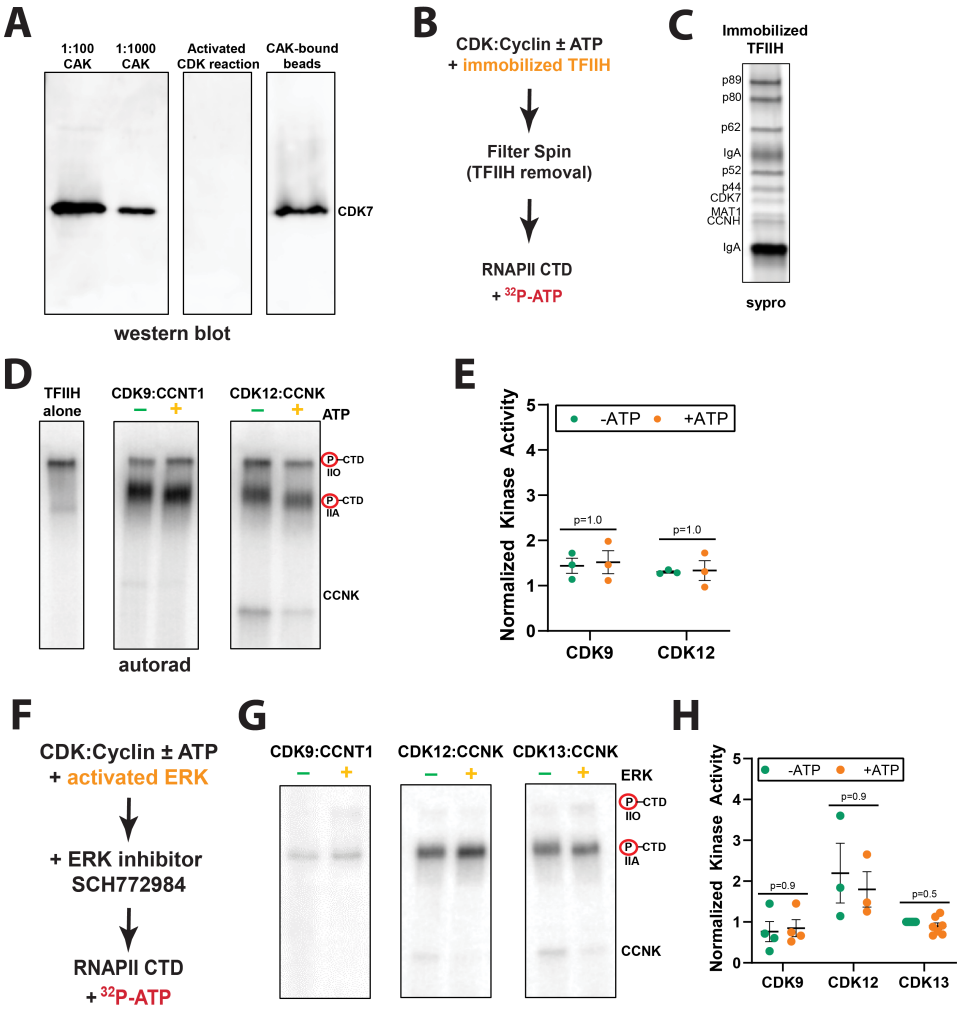

Supplemental Figure 13. Additional kinase assay details; CDK7 cannot activate CDK9 or CDK12 within TFIIH, ERK cannot activate CDK9, CDK12, or CDK13

(A) Confirmation that the CAK was effectively depleted from the kinase activation assays with the RNAPII CTD (representative western blot).

(B) Experimental overview; CDK:cyclin complexes were incubated with immobilized TFIIH ± ATP, TFIIH removed by filter spin, and CDK:cyclin complexes tested for activity towards the RNAPII CTD.

(C) Immobilized TFIIH on Protein A agarose beads, SYPRO Ruby stained.

(D) *In vitro* activation assays with TFIIH as activating kinase ± ATP (instead of the CAK), illustrating CDK7 in the context of TFIIH does not activate, in contrast to CDK7 within the CAK (**Fig. 6**).

(E) Quantitation of data from panel D, across biological replicates (n=3), with autorad signal normalized to TFIIH alone conditions; p=0.1 for CDK9 and CDK12.

(F) Experimental overview. CDK:cyclin complexes were incubated with ERK ± ATP, ERK was then inhibited with the ERK-specific inhibitor SCH772984, and CDK:cyclin complexes tested for activity towards the RNAPII CTD.

(G) *In vitro* kinase assays performed with ERK as the activating kinase ± ATP (instead of the CAK), showing ERK does not function as an activator of CDK9 or CDK12/13.

(H) Quantitation of data from panel G, across biological replicates (n=3), with autorad signal normalized to CDK13 –ATP pre-treatment conditions; p-values as shown.

Table S1. Summary of KiNativ results with SY-351 at 1 μM and 0.2 μM concentration.

Kinase(s)	Reference	Sequence	Labeling Site	1 µM SY-351	0.2 µM SY-351
CDK7	UniRef100_P50613	DLKPNNLLLDENGVLK	Lys2	98	92
CRK7	UniRef100_Q9NYV4	DIKCSNILLNNSGQIK	Lys2	81	36
JNK1, JNK2, JNK3	UniRef100_P45983, UniRef100_P53779, UniRef100_P45984	DLKPSNIVVK	Lys2	71	40
CHED	UniRef100_Q14004	DIKCSNILLNNR	Lys2	65	35
GSK3A	UniRef100_P49840	DIKPQNLLVDPDTAVLK	Lys2	54	8
GSK3B	UniRef100_P49841	DIKPQNLLLDPDTAVLK	Lys2	51	16
RSK4 domain1	UniRef100_Q9UK32	DLKPENILLDEIGHIK	Lys2	46	11
PKD3	UniRef100_O94806	DVAIKVIDK	Lys1	45	19
PKD3	UniRef100_O94806	NIVHCDLKPENVLLASAEPFPQVK	Lys2	43	18
PIP4K2C	UniRef100_Q8TBX8	VKELPTLKDMDFLNK	ATP	34	-7
PCTAIRE1, PCTAIRE3	UniRef100_Q00536, UniRef100_Q07002	DLKPQNLLINER	Lys2	33	16
RSK2 domain1	UniRef100_P51812	LTDFGLSKESIDHEKK	Activation Loop	33	14
PIP4K2C	UniRef100_Q8TBX8	TLVIKEVSSEDIADMHSNLSNYHQYIVK	ATP	33	-1
PKD2	UniRef100_Q9BZL6	DVAVKVIDK	Lys1	31	24
CDK9	UniRef100_P50750	DMKAANVLITR	Lys2	29	-11
PKCa, PKCb	UniRef100_P05771, UniRef100_P17252	DLKLDNVMLDSEGHIK	Lys2	28	2
TLK1	UniRef100_Q9UKI8	YAAVKIHQLNK	Lys1	28	16
PCTAIRE2, PCTAIRE3	UniRef100_Q00537, UniRef100_Q07002	SKLTENLVALKEIR	Lys1	26	4
RSK2 domain1	UniRef100_P51812	VLGQGSFGKVFLVK	ATP Loop	25	-7
PCTAIRE2	UniRef100_Q00537	DLKPQNLLLINEK	Lys2	24	4
GCN2	UniRef100_Q9P2K8	LDGCCYAVKR	Lys1	23	19
MAP2K6	UniRef100_P52564, UniRef100_L5KNH7	HVPSGQIMAVKR	Lys1	22	8
NEK4	UniRef100_P51957	DLKTQNVFLTR	Lys2	22	9
FER	UniRef100_P16591	QEDGGVYSSSGLKQIPIK	Activation Loop	21	5
RSK1 domain1, RSK2 domain1, RSK3 domain1	UniRef100_P51812, UniRef100_Q15418, UniRef100_Q15349	DLKPENILLDEEGHIK	Lys2	20	-11
TAO1, TAO3	UniRef100_Q7L7X3, UniRef100_Q9H2K8	DIKAGNILLTEPGQVK	Lys2	19	12
RSK2 domain1	UniRef100_P51812	DLKPENILLDEEGHIKLTDFGLSKESIDHEK	Lys2	19	5
CDK5	UniRef100_Q00535	NRETHEIVALKR	Lys1	18	13
RON	UniRef100_Q04912	IQCAIKSLSR	Lys1	18	13
PI4KB	UniRef100_Q9UBF8	VPHTQAVVLNSKDK	ATP	18	14
PKN2	UniRef100_Q16513	DLKLDNLLLDTEGFVK	Lys2	18	-13
Erk5	UniRef100_Q13164	DLKPSNLLVNENCELK	Lys2	18	4
MST4, YSK1	UniRef100_O00506, UniRef100_Q9P289	DIKAANVLLSEQGDVK	Lys2	18	16
CaMK2a, CaMK2b, CaMK2d, CaMK2g	UniRef100_Q53H78, UniRef100_Q13557, UniRef100_Q13555, UniRef100_Q9UQM7	DLKPENLLLASK	Lys2	17	5
TAO2	UniRef100_Q9UL54	DVKAGNILLSEPGLVK	Lys2	17	9
EphB4	UniRef100_P54760	FLEENSSDPTYTSSLGGKIPIR	Activation Loop	17	7
YANK3	UniRef100_Q86UX6	DVKPDNILLDER	Lys2	16	-8
MAP2K6	UniRef100_P52564, UniRef100_L5KNH7	DVKPSNVLINALGQVK	Lys2	16	2
TLK2	UniRef100_Q86UE8	YVAVKIHQLNK	Lys1	16	8
MLK3	UniRef100_Q16584	GELVAVKAAR	Lys1	16	19
MLK2	UniRef100_Q02779	DLKSINILILEAIENHNLADTVLK	Lys2	16	-12
CRK	UniRef100_Q8IZL9	DLKPANLLISASGQLK	Lys2	16	7

PI4KA, PI4KAP2	UniRef100_A4QPH2, UniRef100_P42356	SGTPMQSAAKAPYLAK	ATP	15	1
NEK1	UniRef100_Q96PY6	DIKSQNIFLTK	Lys2	15	2
LYN	UniRef100_P07948	VAVKTLKPGTMSVQAFLEEANLMK	Lys1	15	-23
p38a	UniRef100_Q16539	DLKPSNLAVNEDCELK	Lys2	15	0
EphA2	UniRef100_P29317	VLEDDPEATYTTSGGKIPIR	Activation Loop	15	14
MAP3K5	UniRef100_Q99683	DIKGDNVLINTYSGVLK	Lys2	15	5
RSK1 domain2	UniRef100_Q15418	DLKPSNILYVDESGNPECLR	Lys2	15	-2
smMLCK	UniRef100_Q15746	QGIVHLDLKPENIMCVNK	Lys2	14	-1
CLK3	UniRef100_P49761	YEIVGNLGEGTFGKVVECLDHAR	ATP Loop	14	-11
GCK	UniRef100_Q12851	DIKGANLLLTLQGDVK	Lys2	14	10
EGFR	UniRef100_P00533	LLGAEEKEYHAEGGKVPIK	Activation Loop	14	18
DNAPK	UniRef100_P78527	KGGSWIQEINVAEK	ATP	14	11
MET	UniRef100_P08581	DMYDKEYYSVHNK	Activation Loop	13	13
IKKe, TBK1	UniRef100_Q14164, UniRef100_Q9UHD2	DIKPGNIMR	Lys2	13	1
IKKb	UniRef100_O14920	WHNQETGEQIAIKQCR	Lys1	13	19
RSK1 domain1	UniRef100_Q15418	DLKPENILLDEEGHIKLTDFGLSKEAIDHEK	Lys2	13	-1
LATS1	UniRef100_O95835	ALYATKTLR	Lys1	13	18
CDK2	UniRef100_P24941	DLKPQNLLINTEGAIK	Lys2	13	1
ULK1	UniRef100_O75385	DLKPQNILLSNPAGR	Lys2	13	9
MAP3K6	UniRef100_O95382	DIKGDNVLINTFSGLLK	Lys2	13	14
PKR	UniRef100_P19525	DLKPSNIFLVDTK	Lys2	13	-8
AMPKa1, AMPKa2	UniRef100_P54646, UniRef100_Q96E92	VAVKILNR	Lys1	13	17
MAST1, MAST2	UniRef100_Q6P0Q8, UniRef100_Q9Y2H9	DLKPDNLLITSMGHIK	Lys2	12	-18
MAP2K1, MAP2K2	UniRef100_P36507, UniRef100_Q02750	KLIHLEIKPAIR	Lys1	12	12
PKD1	UniRef100_Q15139	DVAIKIIDK	Lys1	12	10
KSR1, KSR2	UniRef100_Q6VAB6, UniRef100_Q8IVT5	SKNVFYDNGK	Activation Loop	12	13
MAP2K3	UniRef100_P46734	HAQSGTIMAVKR	Lys1	12	0
TLK2	UniRef100_Q86UE8	YLNEIKPPIIHYDLKPGNILLVNGTACGEIK	Lys2	12	7
NEK8	UniRef100_Q86SG6	DLKTQNILLDK	Lys2	12	6
MAP3K4	UniRef100_Q9Y6R4	DIKGANIFLTSSGLIK	Lys2	12	11
MAP2K4	UniRef100_P45985	MVHKPSGQIMAVKR	Lys1	11	1
CDK5	UniRef100_Q00535	DLKPQNLLINR	Lys2	11	7
STLK6	UniRef100_Q9C0K7	HTPTGTLVTIKITNLENCNEER	Lys1	11	-1
IKKa	UniRef100_O15111	DLKPENIVLQDVGGK	Lys2	11	5
p38d, p38g	UniRef100_O15264, UniRef100_P53778	DLKPGNLAVNEDCELK	Lys2	11	4
AMPKa1, AMPKa2	UniRef100_P54646, UniRef100_Q96E92	DLKPENVLLDAHMNAK	Lys2	11	-6
MAP2K3	UniRef100_P46734	DVKPSNVLINK	Lys2	11	12
AurA	UniRef100_O14965	DIKPENLLLGSAGELK	Lys2	11	6
NEK6, NEK7	UniRef100_Q8TDX7, UniRef100_Q9HC98	DIKPANVFITATGVVK	Lys2	11	1
MLK1	UniRef100_P80192	DLKSSNILILQK	Lys2	11	2
ZAK	UniRef100_Q9NYL2	WISQDKEVAVKK	Lys1	10	14
MPSK1	UniRef100_O75716	LGEGGFSYVDLVEGLHDGHFYALKR	Lys1	10	2
eEF2K	UniRef100_O00418	YIKYNSNSGFVR	ATP	10	8
FAK	UniRef100_Q05397	YMEDSTYYKASK	Activation Loop	10	-10
CDK2	UniRef100_P24941	LTGEVVALKK	Lys1	10	2
MST1, MST2	UniRef100_Q13188, UniRef100_Q13043	DIKAGNILLNTEGHAK	Lys2	10	3

MAP2K7	UniRef100_O14733	DVKPSNILLDER	Lys2	10	3
EphB2	UniRef100_P29323	FLEDDTSDPTYTSALGGKIPIR	Activation Loop	10	-1
ILK	UniRef100_Q13418	ISMADVKFSFQCPGR	Protein Kinase Domain	9	-2
CDC2	UniRef100_Q5H9N4	DLKPQNLLIDDK	Lys2	9	16
PKR	UniRef100_P19525	IGDFGLVTSLKNDGKR	Activation Loop	9	-7
GCN2	UniRef100_Q9P2K8	DLKPVNIFLDSDDHVK	Lys2	9	-8
PRP4	UniRef100_Q13523	AAGIGKDFKENPNLR	Protein Kinase Domain	9	19
ULK3	UniRef100_D3DW67	NISHLDLKPQNILLSSLEKPHLK	Lys2	9	14
PKD1, PKD2	UniRef100_Q9BZL6, UniRef100_Q15139	NIVHCDLKPENVLLASADPFPQVK	Lys2	9	-3
ULK3	UniRef100_D3DW67	EVVAIKCVAK	Lys1	9	15
MLK3	UniRef100_Q16584	DLKSNNILLLQPIESDDMEHK	Lys2	9	-19
NEK9	UniRef100_Q8TD19	RTEDDSLVVWKEVDLTR	Lys1	9	1
RSK1 domain1	UniRef100_Q15418	LTDFGLSKEAIDHEKK	Activation Loop	8	-2
IRE1	UniRef100_O75460	DLKPHNILISMPNAHGK	Lys2	8	-4
NDR1	UniRef100_Q15208	DIKPDNLLLDSK	Lys2	8	7
LATS2	UniRef100_Q9NRM7	DIKPDNILIDLDGHIK	Lys2	8	6
TAK1	UniRef100_O43318	DLKPPNLLLVAGGTVLK	Lys2	8	9
ZC1/HGK, ZC2/TNIK, ZC3/MINK	UniRef100_O95819, UniRef100_Q9UKE5, UniRef100_Q8N4C8	DIKGQNVLLTENAEVK	Lys2	8	4
CK2a2	UniRef100_P19784	DVKPHNVMIDHQQK	Lys2	7	8
MARK1, MARK2	UniRef100_Q7KZI7, UniRef100_Q9P0L2	EVAVKIIDK	Lys1	7	5
IRAK1	UniRef100_P51617	AIQFLHQDSPSLIHGDIKSSNVLLDER	Lys2	7	-2
PITSLRE	UniRef100_P21127	DLKTSNLLLSHAGILK	Lys2	7	-5
FER	UniRef100_P16591	TSVAVKTCKEDLPQELK	Lys1	7	13
GPRK5	UniRef100_P34947	DLKPENILLDDYGHIR	Lys2	7	-10
MAP2K4	UniRef100_P45985	DIKPSNILLDR	Lys2	7	6
MAP3K1	UniRef100_Q13233	DVKGANLLIDSTGQR	Lys2	6	11
SGK2	UniRef100_Q9HBY8	KSDGAFYAVKVLQK	Lys1	6	3
CDC2	UniRef100_Q5H9N4	DLKPQNLLIDDKGTIK	Lys2	6	6
ABL, ARG	UniRef100_P00519, UniRef100_P42684	YSLTVAVKTLKEDTMEVEEFLK	Lys1	6	5
MSK1 domain1	UniRef100_O75582	DIKLENILLDSNGHVVLTDFGLSK	Lys2	6	14
MAP3K2, MAP3K3	UniRef100_Q9Y2U5, UniRef100_Q99759	DIKGANILR	Lys2	6	10
PIK3CB	UniRef100_P42338	VFGEDSVGVIFKNGDDLRQDMLTLQMLR	ATP	6	3
AMPKa1	UniRef100_Q96E92	IGHYILGDTLGVGTFGKVK	ATP Loop	6	-1
MST3	UniRef100_Q9Y6E0	DIKAANVLLSEHGEVK	Lys2	6	2
CASK	UniRef100_O14936	ETGQQFAVKIVDVAK	Lys1	6	-13
NDR1	UniRef100_Q15208	DTGHVYAMKILR	Lys1	6	-4
NDR2	UniRef100_Q9Y2H1	DIKPDNLLLDAK	Lys2	6	0
SLK	UniRef100_Q9H2G2	AQNKETSVLAAAKVIDTK	Lys1	6	0
IKKb	UniRef100_O14920	DLKPENIVLQQGEQR	Lys2	6	3
CHK2	UniRef100_O96017	DLKPENVLLSSQEEDCLIK	Lys2	6	-5
MAP2K1, MAP2K2	UniRef100_P36507, UniRef100_Q02750	DVKPSNILVNSR	Lys2	6	5
MASTL	UniRef100_Q96GX5	GAFGKVYLGQK	ATP Loop	5	-2
MRCKb	UniRef100_Q9Y5S2	DIKPDNVLLDVNGHIR	Lys2	5	-3
MAP2K1	UniRef100_Q02750	IMHRDVKPSNILVNSR	Lys2	5	1
PIP5K3	UniRef100_Q9Y2I7	GGKSGAAFYATEDDRFILK	ATP	5	7

NuaK1	UniRef100_O60285	DLKLENILLDDNCNIK	Lys2	5	8
SNRK	UniRef100_Q9NRH2	DLKPENVVFFEK	Lys2	5	-8
ROCK1, ROCK2	UniRef100_O75116, UniRef100_Q13464	DVKPDNMLLDK	Lys2	5	-2
CDK11, CDK8	UniRef100_P49336, UniRef100_Q9BWU1	DLKPANILVMGEGPER	Lys2	5	-22
RSK2 domain2	UniRef100_P51812	DLKPSNILYVDESGNPESIR	Lys2	5	-5
STLK3	UniRef100_Q9UEW8	DLKAGNILLGEDGSVQIADFGVSAFLATGGDVTR	Lys2	4	16
TGFbR2	UniRef100_P37173	DLKSSNILVK	Lys2	4	-7
Erk2	UniRef100_P28482	DLKPSNLLLNTTCDLK	Lys2	4	0
FRAP	UniRef100_P42345	IQSIAPSLQVITSKQRPR	ATP	4	3
MASTL	UniRef100_Q96GX5	LYAVKVVK	Lys1	4	14
JAK1 domain2	UniRef100_P23458	YDPEGDNTGEQVAVKSLKPESGGNHIADLKK	Lys1	4	21
TYK2 domain2	UniRef100_P29597	IGDFGLAKAVPEGHEYYR	Activation Loop	4	-3
FRK	UniRef100_P42685	HEIKLPVK	Activation Loop	4	18
MAP3K15, MAP3K5, MAP3K6	UniRef100_Q99683, UniRef100_O95382, UniRef100_Q6ZN16	IAIKEIPER	Lys1	3	3
SLK	UniRef100_Q9H2G2	DLKAGNILFTLDGDIK	Lys2	3	6
MAST3	UniRef100_O60307	DLKPDNLLITSLGHIK	Lys2	3	-3
JAK1	UniRef100_P23458	QLASALSYLEDKDLVHGNVCTKNLLLAR	Protein Kinase Domain	3	-15
CaMK1a	UniRef100_Q14012	LVAIKCIAK	Lys1	3	-1
MARK2, MARK3	UniRef100_P27448, UniRef100_Q7KZI7	DLKAENLLLDADMNIK	Lys2	3	-8
Wnk1, Wnk2, Wnk3	UniRef100_Q9Y3S1, UniRef100_D3DUP1, UniRef100_Q9BYP7	DLKCDNIFITGPTGSVK	Lys2	3	4
p70S6K, p70S6Kb	UniRef100_Q9UBS0, UniRef100_P23443	GGYGKVFQVR	ATP Loop	3	-8
OSR1	UniRef100_C9JIG9, UniRef100_O95747	DVKAGNILLGEDGSVQIADFGVSAFLATGGDITR	Lys2	3	14
AKT2, AKT3	UniRef100_Q9Y243, UniRef100_P31751	GTFGKVILVR	ATP Loop	3	5
PEK	UniRef100_Q9NZJ5	DLKPSNIFFTMDDVVK	Lys2	3	-16
LATS1	UniRef100_O95835	DIKPDNILIDR	Lys2	3	1
GCK	UniRef100_Q12851	DTVTSELAAVKIVK	Lys1	3	-13
CK1g2	UniRef100_P78368	DVKPENFLVGRPGTK	Lys2	3	3
MAP3K2	UniRef100_Q9Y2U5	ELAVKQVQFDPDSPETSKEVNALECEIQLLK	Lys1	2	3
PAK4	UniRef100_O96013	DIKSDSILLTHDGR	Lys2	2	-9
KHS2	UniRef100_Q8IVH8	DIKGANILLTDNGHVK	Lys2	2	7
PIP4K2A	UniRef100_P48426	AKELPTLKDNDFINEGQK	ATP	2	7
p70S6Kb	UniRef100_Q9UBS0	DLKPENIMLSSQGHIK	Lys2	2	-3
ACK	UniRef100_Q07912	TVSVAVKCLKPDVLSQPEAMDDFIR	Lys1	2	-13
MLK4	UniRef100_Q5TCX8	DLKSSNILLLEK	Lys2	2	-5
FAK	UniRef100_Q05397	CIGEGQFGDVHQGIYMSPENPALAVAIKTCK	Lys1	2	-24
PKCi	UniRef100_P41743	DLKLDNVLLDSEGHIK	Lys2	2	14
CaMK1d	UniRef100_Q8IU85	LFAVKCIPK	Lys1	2	2
MST2	UniRef100_Q13188	ESGQVVAIKQVPVESDLQEIIK	Lys1	1	-4
MSK2 domain1	UniRef100_O75676	DLKLENVLLDSEGHIVLTDFGLSK	Lys2	1	2
TLK1	UniRef100_Q9UKI8	YLNEIKPPIIHYDLKPGNILLVDGTACGEIK	Lys2	1	-6
Erk1	UniRef100_P27361	DLKPSNLLINTTCDLK	Lys2	1	2
Wnk1, Wnk2, Wnk4	UniRef100_Q96J92, UniRef100_Q9Y3S1, UniRef100_D3DUP1	IGDLGLATLKR	Activation Loop	1	-2
BRAF	UniRef100_P15056	DLKSNNIFLHEDLTVK	Lys2	1	3
CLK1	UniRef100_P49759	LTHTDLKPENILFVQSDYTEAYNPK	Lys2	1	4

KHS1	UniRef100_Q9Y4K4	DIKGANILLTDHGDVK	Lys2	0	6
PAN3	UniRef100_Q58A45	VMDPTKILITGK	ATP	0	-5
p38a	UniRef100_Q16539	QELNKTIWEVPER	Protein Kinase Domain	0	6
SGK3	UniRef100_Q96BR1	FYAVKVLQK	Lys1	0	-5
LOK	UniRef100_O94804	NKETGALAAAKVIETK	Lys1	0	1
NEK9	UniRef100_Q8TD19	DIKTLNIFLTK	Lys2	0	-1
MST1	UniRef100_Q13043	ETGQIVAIKQVPVESDLQEIIK	Lys1	0	1
SRC	UniRef100_P12931	VAIKTLKPGTMSPEAFLQEAQVMKK	Lys1	0	-8
AurA, AurB, AurC	UniRef100_O14965, UniRef100_Q9UQB9, UniRef100_Q96GD4	GKFGNVYLAR	ATP Loop	-1	-4
MARK2	UniRef100_Q7KZI7	EVAVKIIDKTQLNSSSLQK	Lys1	-1	3
PLK1	UniRef100_P53350	CFEISDADTKEVFAGKIVPK	Lys1	-1	-12
MARK3	UniRef100_P27448	EVAIKIIDKTQLNPTSLQK	Lys1	-1	0
AurA	UniRef100_O14965	FILALKVLFK	Lys1	-1	-1
CHK1	UniRef100_B4DT73	DIKPENLLLDER	Lys2	-1	4
CLK2	UniRef100_P49760	LTHTDLKPENILFVNSDYELTYNLEK	Lys2	-1	-9
ILK	UniRef100_Q13418	WQGNDIVVKVLK	Lys1	-1	-9
SRPK1, SRPK2	UniRef100_P78362, UniRef100_Q96SB4	FVAMKVVK	Lys1	-2	8
p70S6K	UniRef100_P23443	DLKPENIMLNHQGHVK	Lys2	-2	-3
CK1d, CK1e	UniRef100_P49674, UniRef100_P48730	DVKPDNFLMGLGKK	Lys2	-2	-19
RSKL1	UniRef100_Q96S38	VLGVIDKVLLVMDTR	ATP	-2	-19
FYN, SRC, YES	UniRef100_P12931, UniRef100_P07947, UniRef100_P06241	QGAKFPIKWTAPEAALYGR	Activation Loop	-2	0
IRAK4	UniRef100_Q9NWZ3	DIKSANILLDEAFTAK	Lys2	-2	-2
NEK7	UniRef100_Q8TDX7	AACLLDGVPVALKK	Lys1	-2	-14
AGK	UniRef100_Q53H12	ATVFLNPAACKGK	ATP	-2	26
PKN1	UniRef100_Q16512	DLKLDNLLLDTEGYVK	Lys2	-2	16
PHKg2	UniRef100_P15735	ATGHEFAVKIMEVTAER	Lys1	-2	-2
MST4	UniRef100_Q9P289	TQQVVAIKIIDLEEAEDEIEDIQQEITVLSQCDSSYVTK	Lys1	-3	6
ATR	UniRef100_Q13535	FYIMMCKPK	ATP	-3	-24
CK2a1	UniRef100_P68400	GGPNIITLADIVKDPVSR	Protein Kinase Domain	-3	-4
CaMK2g	UniRef100_Q13555	TSTQEYAAKIINTK	Lys1	-3	-1
EGFR	UniRef100_P00533	IPVAIKELR	Lys1	-3	-3
CK1a	UniRef100_P48729	DIKPDNFLMGIGR	Lys2	-3	-24
PRPK	UniRef100_Q96S44	FLSGLELVKQGAEAR	ATP Loop	-3	-5
NuaK2	UniRef100_Q9H093	LVAIKSIR	Lys1	-3	-4
ITPK1	UniRef100_Q13572	ESIFFNSHNVSKPESSSVLTELDKIEGVFERPSDEVIR	ATP	-4	1
NuaK1	UniRef100_O60285	VVAIKSIR	Lys1	-4	9
SMG1	UniRef100_Q96Q15	DTVTIHSVGGTITILPTKTKPK	ATP	-4	3
KHS2	UniRef100_Q8IVH8	NVNTGELAAIKVIK	Lys1	-4	0
LOK	UniRef100_O94804	DLKAGNVLMTLEGDIR	Lys2	-4	-15
MARK3, MARK4	UniRef100_Q96L34, UniRef100_P27448	EVAIKIIDK	Lys1	-4	-9
JAK1 domain2	UniRef100_P23458	IGDFGLTKAIETDKEYYTVK	Activation Loop	-4	-16
CHK1	UniRef100_B4DT73	LSKGDGLEFK	Protein Kinase Domain	-4	-1
ABL, ARG	UniRef100_P00519, UniRef100_P42684	LMTGDTYTAHAGAKFPIK	Activation Loop	-5	-17
DNAPK	UniRef100_P78527	EHPFLVKGGEDLR	ATP	-5	0

NDR2	UniRef100_Q9Y2H1	DTGHIYAMKILR	Lys1	-5	-2
PRP4	UniRef100_Q13523	CNILHADIKPDNILVNESK	Lys2	-6	1
TBK1	UniRef100_Q9UHD2	TGDLFAIKVFNNISFLRPVDVQMR	Lys1	-7	-1
HER3/ErbB3	UniRef100_P21860	GVWIPEGESIKIPVCIKVIEDK	Lys1	-7	20
MAP2K5	UniRef100_Q13163	DVKPSNMLVNTR	Lys2	-7	3
SRC	UniRef100_P12931	VAIKTLKPGTMSPEAFLQEAQVMK	Lys1	-8	-21
MST3	UniRef100_Q9Y6E0	VVAIKIIDLEEAEDEIEDIQQEITVLSQCDSPYVTK	Lys1	-8	-8
SRPK1	UniRef100_Q96SB4	IIHTDIKPENILLSVNEQYIR	Lys2	-8	-8
CSK	UniRef100_P41240	VSDFGLTKEASSTQDTGKLPVK	Activation Loop	-8	-6
CHK2	UniRef100_O96017	VAIKIISK	Lys1	-8	8
SMG1	UniRef100_Q96Q15	SYPYLFKGLEDLHLDER	ATP	-9	-13
KHS1	UniRef100_Q9Y4K4	NVHTGELAAVKIIK	Lys1	-9	-4
LRRK2	UniRef100_Q5S007	DLKPHNVLLFTLYPNAAIIAK	Lys2	-9	-9
PKN1	UniRef100_Q16512	VLLSEFRPSGELFAIKALK	Lys1	-9	-15
ARAF	UniRef100_P10398	DLKSNNIFLHEGLTVK	Lys2	-10	-11
MLKL	UniRef100_Q8NB16	APVAIKVFK	Lys1	-10	-3
CaMK2d	UniRef100_Q13557	IPTGQEYAAKIINTKK	Lys1	-10	-1
PIK3C3	UniRef100_Q8NEB9	TEDGGKYPVIFKHGDDLRQDQLILQIISLMDK	ATP	-10	-6
HER2/ErbB2	UniRef100_P04626	LLDIDETEYHADGGKVPIK	Activation Loop	-12	-18
NEK3	UniRef100_P51956	SKNIFLTQNGK	Activation Loop	-13	-11
EphA2	UniRef100_P29317	EVPVAIKTLK	Lys1	-13	-8
PKCi	UniRef100_P41743	IYAMKVVK	Lys1	-13	0
MAPKAPK3	UniRef100_Q16644	QVLGLGVNGKVLECFHR	ATP Loop	-14	-14
DGKA	UniRef100_P23743	IDPVPNTHPLLVFVNPKSGGK	ATP	-18	4
STLK6	UniRef100_Q9C0K7	SIKASHILISGDGLVTLSGLSHLHSLVK	Lys2	-21	-5
MELK	UniRef100_Q14680	DLKPENLLFDEYHK	Lys2	-21	-47
PRP4	UniRef100_Q13523	ANQEVAVKIIR	Lys1	-23	-49
PI4KB	UniRef100_Q9UBF8	LLSVIVKCGDDLRQELLAFQVLK	ATP	-25	-10
SGK3	UniRef100_Q96BR1	IVYRDLKPENILLDSVGHVVLTDFGLCK	Lys2	-27	-7
HER2/ErbB2	UniRef100_P04626	GIWIPDGENVKIPVAIKVLR	Lys1	-34	-41
LYN	UniRef100_P07948	EGAKFPIKWTAPEAINFGCFTIK	Activation Loop	-54	-43

Uniprot Accession	Protein	Counts of replicate with Ratio≥3	Average #unique peptide	Probes ≥ 2 replicate	Probes 1 replicate	Probe @ 100 nM
Q9NYV4-1	Cyclin-dependent kinase 12	24	2.5	all		yes
A0A024R8S5	Protein disulfide-isomerase	21	35.1	all		yes
J3KNF8	Cytochrome b5 type B	19	4.1	all		yes
Q99808-2	Isoform 2 of Equilibrative nucleoside transporter 1	17	3.0	all		yes
Q14004-1	Cyclin-dependent kinase 13	17	1.8	all		yes
A0A087WYF7	MICOS complex subunit	12	2.3	4305, 4334	4241	yes
A0A0S2Z3F9	Cyclin-dependent kinase 7	12	1.8	all		yes
Q53G34	Mitochondrial carrier homolog 2 variant	10	4.1	all		yes
Q9NQC3	Reticulon-4	9	2.3	4305, 4334	4241	yes
A0A024R6P6	Chromosome 14 open reading frame 129	8	1.9	4305, 4334	4241	yes
A0A024R8G6	Sjogren's syndrome nuclear autoantigen 1	7	2.0	4305		yes
B4DPG9	cDNA FLJ59630	5	1.9	4305	4241	yes
A0A087WT44	Heme oxygenase 2	11	5.3	all		no
Q9BTY7	Protein HGH1 homolog	10	5.7	4305, 4334		no
Q15418-2	Isoform 2 of Ribosomal protein S6 kinase alpha-1	9	4.9	4305, 4334	4241	no
Q53GI2	Testis expressed sequence 264 variant	8	2.3	4305, 4334		no
Q8TCD1	UPF0729 protein C18orf32	8	1.2	4305, 4334		no
Q9NQC3-2	Isoform 2 of Reticulon-4	7	3.4	4305, 4334	4241	no
Q8NBS9-1	Thioredoxin domain-containing protein 5	5	5.3	4305	4241, 4334	no
O43765	Small glutamine-rich tetratricopeptide repeat-	5	4.2	4305	4241, 4334	no
O00154	Cytosolic acyl coenzyme A thioester hydrolase	5	3.3	4305, 4334	4241	no
Q6L8Q7-1	2',5'-phosphodiesterase 12	5	3.3	4334	4241, 4305	no
A0A024R0C0	Choline/ethanolamine phosphotransferase 1	5	1.0	4305	4334	no
P49327	Fatty acid synthase	4	20.3	4334		yes
P12081	Histidine--tRNA ligase, cytoplasmic	4	7.4	4305		yes
Q15084-2	Isoform 2 of Protein disulfide-isomerase A6	4	7.3	4305	4334	no
Q8NBX0	Saccharopine dehydrogenase-like oxidoreductase	4	3.8	4305	4334	no
Q9UBB4-1	Ataxin-10	4	3.3	4305	4241	no
A0A0S2Z5D6	Abhydrolase domain containing 5 isoform 1	4	1.0	4334	4305	no
P49841-2	Isoform 2 of Glycogen synthase kinase-3 beta	4	1.0	4305	4334	no
Q01804-1	OTU domain-containing protein 4	4	1.0	4305	4334	no
A0A0S2Z5A6	Transporter 1 ATP-binding cassette sub-family B	4	1.0	4305	4334	no
A0A024R3C7	Ataxia telangiectasia mutated (Includes	4	1.0	4305	4334	no
Q59FM4	Scavenger receptor class B member 1 variant	3	1.6	4334	4305	yes
A0A0S2Z4K2	CCHC-type zinc finger nucleic acid binding protein	3	3.9	4334	4305	no
P16615	Sarcoplasmic/endoplasmic reticulum calcium ATPase	3	2.9	4305		no
Q6PJG6-1	BRCA1-associated ATM activator 1	3	2.1	4305	4241	no
B7Z6M0	Peptidylprolyl isomerase	3	1.6	4305	4334	no
P15814	Immunoglobulin lambda-like polypeptide 1	3	1.3	4305	4334	no
A0A024QZN9	Voltage-dependent anion channel 2	2	9.9	4305		yes
Q9NX40	OCIA domain-containing protein 1	2	2.2	4305		no
Q9UG56-3	Phosphatidylserine decarboxylase proenzyme,	2	1.7	4305		no
Q13257-1	Mitotic spindle assembly checkpoint protein MAD2A	2	1.0	4334		no
B7Z351	Secreted phosphoprotein 1 variant 6	2	1.0	4305		no
Q92621	Nuclear pore complex protein Nup205	2	1.0	4305		no
A0A0A0MTS7	Titin	2	1.0	4334		no

Table S2. Ranked list of 46 proteins identified as SY-351 interactors in the ABPP experiments. The primary ranking criterion was the number of independent samples, of 27 total, for which corresponding peptide peaks were three-fold or larger in the presence of SY-351 (ratio of heavy:light peaks ≥ 3). In addition, proteins had a higher rank if they were identified in at least one incubation with 100 nM probe. In cases where proteins were equally strongly identified by these two criteria, the protein with a higher average number of unique peptides (sum of number of unique peptides from all samples in which at least one unique peptide was identified divided by the number of samples giving at least one unique peptide) was ranked higher. **CDK12 (1490 residues) and CDK13 (1512 residues) are favored in this ranking (vs. CDK7; 346 residues) because they are much larger proteins.**

Gene	Sites	CDK7	CDK8	CDK9-Decker	CDK9-Sanso	CDK12/13
SF3B1	T326, T434, S349, T223, T227, T350, T273, T303, T313	+				+
SF3B1	T142, T267, T278				+	+
SF3B1	T227	+	+			+
SF3B1	S129		+			+
U2AF2	S79	+		+		
RBM25	S677	+		+		+
SRRM1	T614, T616			+		+
SRRM2	S1694	+		+		
SRRM2	S398		+	+		
CASC3	S125	+				+
CASC3	S148		+	+		
THRAP3	S379	+	+	+		
THRAP3	S575	+	+			
SRSF9	S216		+	+		
DGCR14	T3	+	+			
PRRC2A	S456	+		+		
PRPF4B	S294		+	+		
ESF1	S694		+			+
DDX21	S71	+	+			+
MATR3	S195, 206	+				+
MEPCE	T213	+			+	+
MEPCE	S217				+	+
CDC5L	T438	+				+
CDC5L	T442	+			+	+
TMPO	S67		+	+		
FAM122B	S119		+	+		
NELFE	S115	+		+		
SUPT5H	S666	+			+	
GATAD2B	S135	+	+			
DIDO1	S1456	+		+		
IRF2BP1	S186		+		+	
FOXK1	S428	+			+	
AGFG1	T177, S181	+				+
SEC22B	S137	+	+			
HUWE1	S2362	+		+		
ARFGEF1	S1566, S1569	+		+		
TBC1D110B	S687	+		+		

Table S3. Summary table for phosphoproteins that contained at least one significantly decreased phospho-site ($q < 0.01$) with SY-351 treatment. Phosphoproteins that have been identified as substrates for CDK7 and other CDK transcriptional kinases are shown in (**+**): CDK8 (Poss et al. 2016), CDK9 (Sanso et al. 2016; Decker et al. 2019), and CDK12/13 (Krajewska et al. 2019).

Table S4. SILAC-MS data (Excel file)

Synthesis of chemical compounds
SY-351 was prepared as described (Hu et al. 2019).

ABPP probes: SY-4241, SY-4305, and SY-4334 were synthesized as outlined below. These compounds inhibited CDK7/CCNH/MAT1 in enzymatic activity assays with IC_{50} values of 295 nM, 42 nM, and 81 nM, respectively with K_m [ATP].

Synthesis of SY-4241:

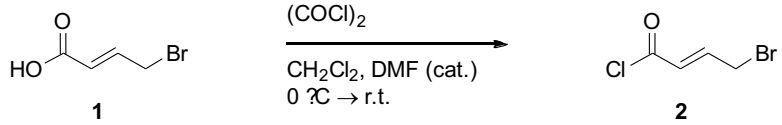

(E)-4-bromobut-2-enoyl chloride (2): Oxalyl chloride (0.264 mL. 3.03 mmol) was added to a stirring solution of (E)-4-bromobut-2-enoic acid (**1**) (500 mg, 3.03 mmol) in dichloromethane (10 mL) and *N*,*N*-dimethylformamide (20 μL) at 0°C and left stirring for 2 hours at room temperature (complete conversion by LCMS by quenching with diethylamine to confirmed the acyl chloride formation). The solution was used as such in the next step.

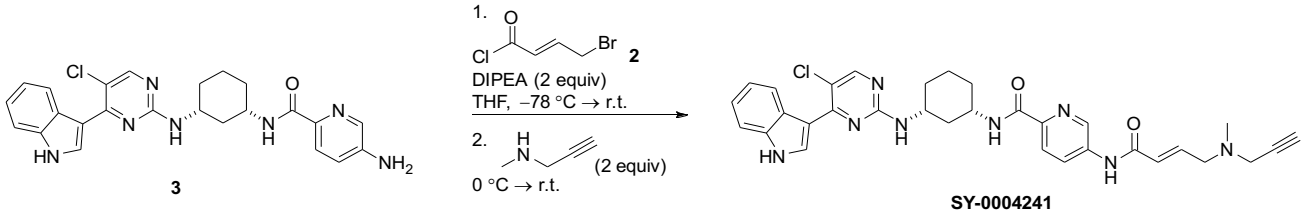

N-((1S,3R)-3-((5-chloro-4-(1H-indol-3-yl)pyrimidin-2-yl)amino)cyclohexyl)-5-((E)-4-(methyl(prop-2-yn-1-yl)amino)but-2-enamido)picolinamide (SY-4241): To a round bottom flask, 5-amino-N-((1S,3R)-3-((5-chloro-4-(1H-indol-3-yl)pyrimidin-2-yl)amino)cyclohexyl)picolinamide (200 mg, 0.43 mmol) was dissolved in tetrahydrofuran (1.45 mL) and cooled to –78 °C. The solution was treated with a freshly made solution of (E)-4-bromobut-2-enoyl chloride (1.45 mL, 0.43 mmol, 0.3 M). The solution was then left to warm to room temperature. After an hour, conversion to the amide was complete. The solution was cooled to 0 °C and *N*-methylpropargylamine (0.073 mL, 0.87 mmol) was added and then left to warm to room temperature. After 1 hour, the solution was diluted with water and extracted twice with 2-methyltetrahydrofuran. The combined organic layer was dried over sodium sulfate and evaporated under vacuum. The crude mixture was purified via reverse phase column chromatography (30 g) using 10 – 70 % MeCN / 10 mM AMF aq as eluent (compound came out with 55%). The pure fractions were combined and volatiles were removed under reduced pressure. The remaining aqueous phase was extracted twice with 2-methyltetrahydrofuran, dried over sodium sulfate, filtered and evaporated under reduced pressure. The crude mixture was then dissolved in EtOAc, dried again over sodium sulfate, filtered and evaporated under reduced pressure. The desired product was obtained in 80 % purity. The impure mixture was then re-purified via reverse phase column chromatography (12 g) using 20 – 60 % MeCN / water as eluent. Pure fractions were combined, frozen and lyophilized for 16 hours. The desired product N-((1S,3R)-3-((5-chloro-4-(1H-indol-3-yl)pyrimidin-2-yl)amino)cyclohexyl)-5-((E)-4-(methyl(prop-2-yn-1-yl)amino)but-2-enamido)picolinamide (**SY-4241**) was obtained as an off-white amorphous solid (34.2 mg, 0.057 mmol) 13 % yield, 97.7 % purity.

LCMS M+H (*m/z*) = 597.2 R_T = 1.56 min (5 – 100 % MeCN / 10 mM AmF aq., 3 min.)
^{1}H NMR (400 MHz, $CDCl_3$) δ 8.66 (s br, 1H), 8.64 – 8.50 (m, 2H), 8.37 (s, 1H), 8.24 – 8.21 (m, 1H), 8.21 – 8.16 (m, J = 4.3 Hz, 2H), 7.89 – 7.76 (m, 1H), 7.46 – 7.41 (m, 1H), 7.38 – 7.34 (m, 1H), 7.33 – 7.29 (m, 3H), 7.05 – 6.96 (m, 1H), 6.19 (d, J = 15.2 Hz, 1H), 5.03 (d, J = 8.2 Hz, 1H), 4.28 – 4.00 (m,

2H), 3.37 (d, J = 2.4 Hz, 2H), 3.28 (dd, J = 5.9, 1.5 Hz, 2H), 2.65 – 2.55 (m, 1H), 2.36 (s, 3H), 2.31 – 2.23 (m, 2H), 2.21 – 2.12 (m, 1H), 1.92 (dd, J = 10.7, 3.4 Hz, 1H), 1.66 – 1.61 (m, 1H), 1.54 – 1.46 (m, 1H), 1.39 – 1.14 (m, 4H).

Synthesis of SY-4305:

Step 1:

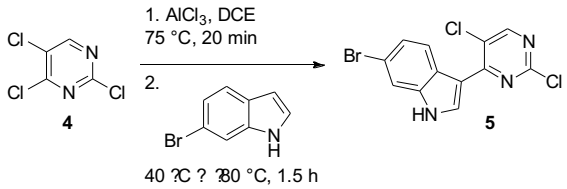

6-bromo-3-(2,5-dichloropyrimidin-4-yl)-1H-indole (5): To a round bottom flask, 2,4,5-trichloropyrimidine (**4**) (1.00 g, 5.45 mmol) was suspended in 1,2-dichloroethane and purged under nitrogen atmosphere. Aluminum trichloride (1.03 g, 5.24 mmol) was then added and the suspension was stirred at 75 °C for 20 min to give a faint orange suspension. After 20 mins, the reaction was cooled to 40 °C and 6-bromoindole (1.03 g, 5.50 mmol) was then added. The flask was then equipped with a condenser and the solution was heated to 80 °C for 1.5 hour. The resulting dark brown suspension was added portion-wise to 100 mL of ice with stirring and the remaining residues were partitioned between a minimum of 2-methyltetrahydrofuran and water (1:1 v/v). Once the ice had completely melted, the resulting solution was extracted twice with 2-methyltetrahydrofuran. The combined organic phase was dried over sodium sulfate, filtered and dried under vacuum. The resulting crude solid (85 % purity) was suspended in 10 mL of tert-butylmethylether, sonicated for 3 minutes and stirred vigorously (500 rpm) for 5 minutes. The solid was filtered, washed with a minimum of tert-butylmethylether (2 mL) and dried under vacuum. The desired product 6-bromo-3-(2,5-dichloropyrimidin-4-yl)-1H-indole (**5**) was obtained as a brown amorphous solid (1.13 g, 3.28 mmol), 63 % yield, 99 % purity.

LCMS: *m/z* (+H$^+$) = 341.9, R_T = 1.95 min (5 – 100 % MeCN / 10 mM AmF aq., 3 min)
^{1}H NMR (400 MHz, DMSO-d_6) δ 12.31 (s br, 1H), 8.76 (s, 1H), 8.72 (d, J = 3.2 Hz, 1H), 8.41 (d, J = 8.7 Hz, 1H), 7.75 – 7.70 (m, 1H), 7.39 (dd, J = 8.7, 1.9 Hz, 1H).

Step 2:

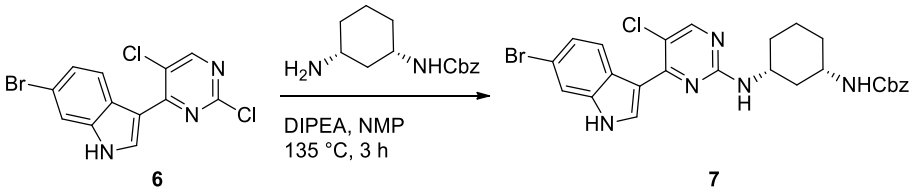

benzyl ((1S,3R)-3-((4-(6-bromo-1H-indol-3-yl)-5-chloropyrimidin-2-yl)amino)cyclohexyl)carbamate (6): To a suspension of 6-bromo-3-(2,5-dichloropyrimidin-4-yl)-1H-indole (0.756 g, 2.20 mmol) in NMP (2.75 mL) was added benzyl ((1S,3R)-3-aminocyclohexyl)carbamate (**5**) (0.574 g, 2.31 mmol) and diisopropylethylamine (1.15 mL, 6.61 mmol). The resulting mixture was heated to 135 °C for 1.5 hours using an oil bath. The reaction was then cooled down to room temperature and added dropwise to an aqueous HCl solution (6.0 mL conc. HCl /50 mL water). The resulting beige suspension was filtered and rinsed with water. The cake was then dried under vacuum, triturated in 50 mL of acetonitrile, filtered, dried again under vacuum. The desired product benzyl ((1S,3R)-3-((4-(6-bromo-1H-indol-3-yl)-5-chloropyrimidin-2-yl)amino)cyclohexyl)carbamate (**6**) was obtained as a brown amorphous solid (0.87 g, 71.52 mmol), 72% yield, 78 % purity.

LCMS: M+H (*m/z*) = 555.9, R_T = 1.95 min (5 – 100 % MeCN / 10 mM AmF aq., 3 min)

Step 3:

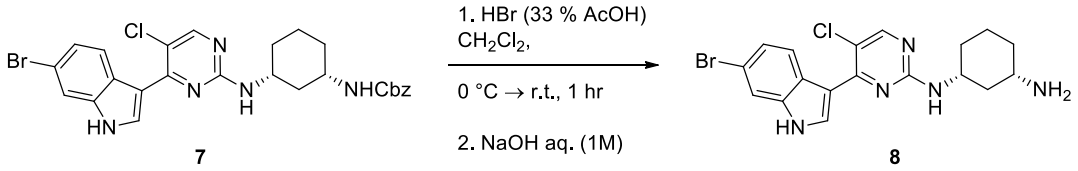

(1R,3S)-N1-(4-(6-bromo-1H-indol-3-yl)-5-chloropyrimidin-2-yl)cyclohexane-1,3-amine (7): To a suspension of benzyl ((1S,3R)-3-((4-(6-bromo-1H-indol-3-yl)-5-chloropyrimidin-2-yl)amino)cyclohexyl)carbamate (**6**) (0.7842 g, 1.41 mmol) in dichloromethane (10 mL) in an ice bath. The mixture was then treated with HBr solution (2.5 mL, 33 % in AcOH). The mixture was allowed to warm to room temperature and left to stir for 2 hours. The mixture was then added portion-wise to *tert*-butylmethylether (100 mL) and left to stir overnight. The next morning, the precipitate was filtered, washed with *tert*-butylmethylether, and dried under vacuum. The desired product (1R,3S)-N^1-(4-(6-bromo-1H-indol-3-yl)-5-chloropyrimidin-2-yl)cyclohexane-1,3-amine ammonium bromide was obtained as amorphous dark yellow solid (0.755 g, 1.51 mmol), 97 % purity. The solid was then suspended in 2-methyltetrahydrofuran and partitioned with NaOH aq (1M) in a separatory funnell. The aqueous phase was extracted twice with 2-methyltetrahydrofuran. The combined organic phase was dried over sodium sulfate, filtered and evaporated under vacuum. The desired product (1R,3S)-N1-(4-(6-bromo-1H-indol-3-yl)-5-chloropyrimidin-2-yl)cyclohexane-1,3-diamine (**7**) was obtained as a brown amorphous solid (0.4942 g, 1.17 mmol), 83 % yield. 90 % purity.

LCMS: M+H (*m/z*) = 420.1, R_T = 1.39 min (5 – 100 % MeCN / 10 mM AmF aq., 3 min)

Step 4:

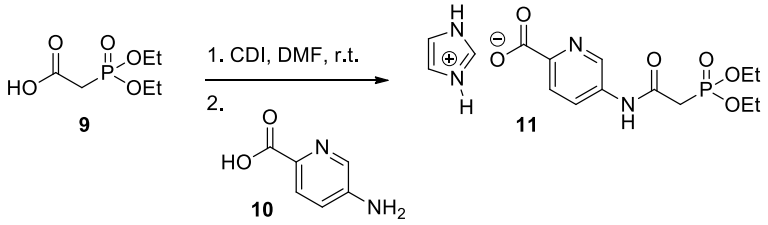

1H-imidazol-3-ium 5-(2-(diethoxyphosphoryl)acetamido)picolinate (10): To a round bottom flask, 2-(diethoxyphosphoryl)acetic acid (**8**) (92.33 g, 471 mmol) was dissolved in *N*,*N*-dimethylformamide (471 mL, 1.0 M) to which was added *N*,*N*-carbonyldiimidazole (77.09 g, 475 mmol) in small portions and the solution is stirred under nitrogen atmosphere. After 60 minutes, 5-aminopyridine-2-carboxylic acid (**9**) (65.02 g, 471 mmol) was added and the solution was left to stir at room temperature overnight. The next morning the precipitate was filtered, washed with acetone (500 mL) and dried under vacuum. The desired product (**10**) was obtained as a white amorphous solid (118 g, 306 mmol), 65 % yield, 99 % purity by LCMS. 95 % purity by ^{1}H NMR; traces of *N*,*N*-dimethylformamide.

LCMS: M+H (*m/z*) = 317.15, R_T = 0.88 min (5 – 100 % MeCN / 10 mM AmF aq., 3 min)
^{1}H NMR (500 MHz, DMSO-d_6) δ 10.67 (s, 1H), 8.78 (dd, J = 2.5, 0.5 Hz, 1H), 8.21 (dd, J = 8.6, 2.5 Hz, 1H), 8.04 (d, J = 8.5 Hz, 1H), 7.67 (s, 1H), 7.03 (d, J = 1.0 Hz, 2H), 5.21 (s br, 1H) 4.23 – 3.93 (m, 4H), 3.16 (d, J = 21.5 Hz, 2H), 1.24 (t, J = 7.1 Hz, 6H).

Step 5:

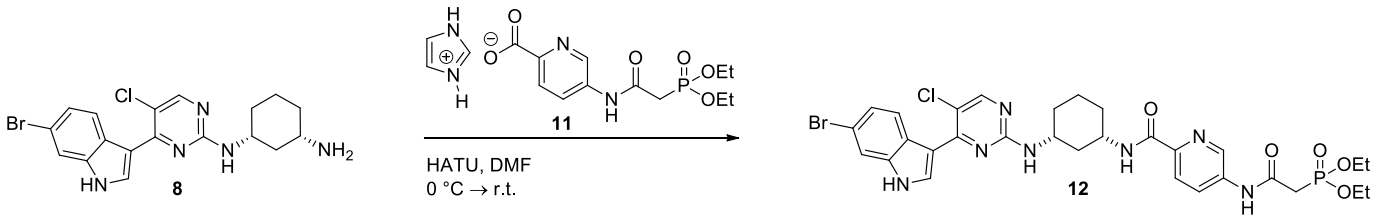

diethyl (2-((6-(((1S,3R)-3-((4-(6-bromo-1H-indol-3-yl)-5-chloropyrimidin-2-yl)amino)cyclohexyl)carbamoyl)pyridin-3-yl)amino)-2-oxoethyl)phosphonate (11): To a round bottom flask, 1H-imidazol-3-ium 5-(2-(diethoxyphosphoryl)acetamido)picolinate (**10**) (0.4948 g, 1.29 mmol) was suspended in N,N-dimethylformamide (2.8 mL). To this solution DIPEA (0.41 mL, 2.34 mmol) was added and the solution was stirred until all was dissolved. The solution was then cooled to 0 °C and 1-[bis(dimethylamino)methylene]-1H-1,2,3-triazolo[4,5-b]pyridinium-3-oxid-hexafluorophosphate (HATU) (0.4895 g, 1.29 mmol) was added. The reaction was stirred under nitrogen atmosphere for 5 minutes and turned bright yellow. Following this, (1R,3S)-N1-(4-(6-bromo-1H-indol-3-yl)-5-chloropyrimidin-2-yl)cyclohexane-1,3-amine (**7**) (0.4924 g, 1.17 mmol) was dissolved in *N,N*-dimethylformamide and added to the solution. The reaction was stirred and left to slowly warmed up to room temperature. After 1h, the resulting mixture was then added dropwise to water (20 mL) and stirred vigorously (>800 rpm). Cold water (10 mL) was then added and the mixture was stirred overnight. The resulting beige precipitate was then filtered, washed with water (50 mL) and dried under vacuum. The product (**11**) was obtained as a yellow amorphous solid (0.713 g, 0.99 mmol) 85 % yield, 79 % purity.

LCMS: M+H (*m/z*) = 717.9, 720.0, 721.0, R_T = 1.69 min (5 – 100 % MeCN / 10 mM AmF aq., 3 min)

Step 6:

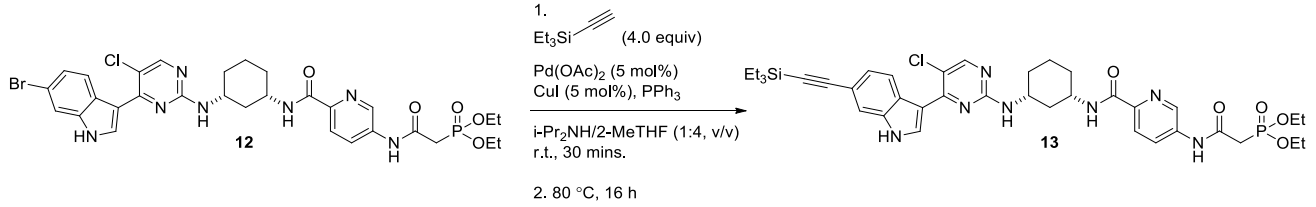

diethyl (2-((6-(((1S,3R)-3-((5-chloro-4-(6-((triethylsilyl)ethynyl)-1H-indol-3-yl)pyrimidin-2-yl)amino)cyclohexyl)carbamoyl)pyridin-3-yl)amino)-2-oxoethyl)phosphonate (12): To a solution of diethyl (2-((6-(((1S,3R)-3-((4-(6-bromo-1H-indol-3-yl)-5-chloropyrimidin-2-yl)amino)cyclohexyl)carbamoyl)pyridin-3-yl)amino)-2-oxoethyl)phosphonate (**11**) (300 mg , 0.417 mmol) in iPr_2NH / THF (4.17 mL, 1:4 v/v) under an nitrogen atmosphere were added catalytic amounts of CuI (2.7 mg, 5 mol%), $Pd(OAc)_2$ (4.7 mg, 5 mol%), and triphenylphosphine (27.4 mg, 25 mol%). The solution was stirred for 30 minutes at room temperature, and then trimethylsilylethyne (234.2 mg, 1.67 mmol) was added under vigorous stirring. The reaction mixture was then heated to 80 °C overnight. After being cooled to room temperature, the mixture was filtered, washed with methanol and concentrated under vacuum. The crude mixture was purified by normal phase column chromatography using 0 – 10 % MeOH / dichloromethane as eluent. The desired product (**12**) was obtained as a white amorphous solid (187 mg, 0.24 mmol), 99 % purity, 58 % isolated yield.

LCMS M+H (*m/z*) = 778.1, 779.0, 781.4, R_T = 2.13 min (5 – 100 % MeCN / 10 mM AmF aq., 3 min)
^{1}H NMR (400 MHz, DMSO-d_6) δ 12.12 (d, J = 142.7 Hz, 1H), 10.62 (s, 1H), 8.77 (dd, J = 12.5, 2.5 Hz, 1H), 8.55 (dd, J = 9.3, 5.8 Hz, 3H), 8.27 (s, 1H), 8.19 (dd, J = 8.6, 2.4 Hz, 1H), 8.02 (dd, J = 8.6, 4.3

Hz, 1H), 7.59 (s, 1H), 7.53 – 7.08 (m, 2H), 4.13 – 3.97 (m, 4H), 3.14 (d, J = 21.5 Hz, 2H), 2.21 (s, 1H), 2.03 (d, J = 40.4 Hz, 1H), 1.82 (s, 2H), 1.62 – 1.35 (m, 3H), 1.21 (dt, J = 14.3, 7.4 Hz, 8H), 1.04 (dd, J = 11.0, 4.7 Hz, 8H), 0.97 (dd, J = 10.2, 5.3 Hz, 1H), 0.76 – 0.58 (m, 6H).

Step 7:

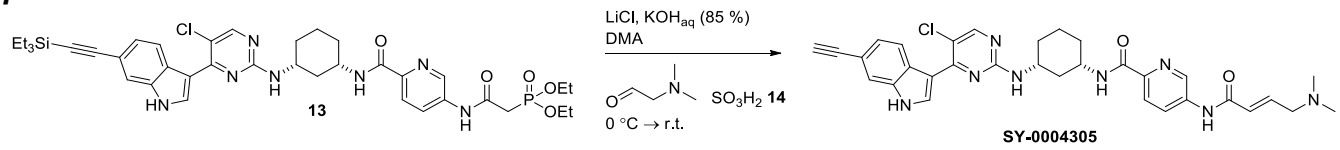

N-((1S,3R)-3-((5-chloro-4-(6-ethynyl-1H-indol-3-yl)pyrimidin-2-yl)amino)cyclohexyl)-5-((E)-4-(dimethylamino)but-2-enamido)picolinamide (SY-4305): To a 10 mL round bottom flask, diethyl (2-((6-(((1S,3R)-3-((5-chloro-4-(6-((triethylsilyl)ethynyl)-1H-indol-3-yl)pyrimidin-2-yl)amino)cyclohexyl)carbamoyl)pyridin-3-yl)amino)-2-oxoethyl)phosphonate (**12**) (187 mg, 0.240 mmol) was dissolved *N,N*-dimethylacetamide (2.40 mL). The reaction was stirred under nitrogen atmosphere. To this solution was added lithium chloride monohydrate (11.2 mg, 0.264 mmol) and the solution was stirred until dissolved. To the solution, 85 % KOH in water (1.15 mL, 24.1 mmol) was added and the reaction was left to stir at room temperature. After 15 minutes, 1.15 mL of *N,N*-dimethylaminoacetaldehyde solution in water (**13**) (0.102 g, 0.601 mmol, 0.52 M) was added dropwise. The reaction was then left to warm to room temperature and was monitored by LCMS until judged complete. The crude solution was then added dropwise to 25 mL of water under vigorous stirring (>500 rpm). The milky solution was then partitioned with 2-methyltetrahydrofuran and extracted twice (2 X 50 mL). The combined organic layer was then dried over sodium sulfate, filtered and evaporated under vacuum. The crude mixture was then purified via reverse phase column chromatography (25 g) using 10 – 60 % MeCN / 10 mM AmF. The pure fractions were then combined, frozen and lyophilized over two days. The desired compound was obtained as a off-white amorphous solid (42 mg, 0.07 mmol), 91 % purity, 29 % isolated yield. The compound was re-purified by reverse-phase column chromatography (12 g) using 20 – 60 % MeCN / 10 mM AmF aq., as eluent. Pure fractions were combined, frozen and lyophilized over two days. The desired compound (**SY-4305**) was obtained as a yellow amorphous solid (26.1 mg, 0.0437 mmol), 99 % purity, 18.19 % isolated yield.

LCMS M+H (*m/z*) = 597.0, 599.0, 600.2, R_T = 1.48 min (5 – 100 % MeCN / 10 mM AMF aq., 3 min.)
^{1}H NMR (400 MHz, DMSO-d_6) δ 11.97 (s, 1H), 10.56 (s, 1H), 8.88 (d, J = 2.4 Hz, 1H), 8.55 (t, J = 5.9 Hz, 3H), 8.35 – 8.17 (m, 3H), 8.01 (d, J = 8.6 Hz, 1H), 7.61 (s, 1H), 7.38 (d, J = 7.5 Hz, 2H), 6.80 (dt, J = 15.4, 5.8 Hz, 1H), 6.29 (d, J = 15.4 Hz, 1H), 4.10 (s, 1H), 3.90 (s, 2H), 3.07 (dd, J = 5.7, 1.3 Hz, 2H), 2.55 (s, 1H), 2.45 (s, 1H), 2.27 – 2.09 (m, 9H), 1.99 (s, 2H), 1.82 (s, 3H), 1.43 (s, 4H), 1.26 (d, J = 21.9 Hz, 1H).

Synthesis of SY-4334:
Step 1:

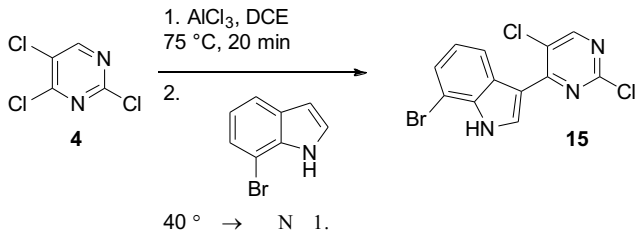

7-bromo-3-(2,5-dichloropyrimidin-4-yl)-1H-indole: To a rbf, 2,4,5-trichloropyrimidine (**4**) (1.00 g, 5.45 mmol) was suspended in 1,2-dichloroethane and purged under nitrogen atmosphere. Aluminum

trichloride (1.03 g, 5.24 mmol) was then added and the suspension was stirred at 75 °C for 20 min to give a faint orange suspension. After 20 minutes, the reaction was cooled to 40 °C and 7-bromoindole (1.03 g, 5.50 mmol) was then added. The flask was then equipped with a condenser and the solution was heated to 80 °C for 1.5 hour.The resulting dark brown suspension was added portion-wise to 100 mL of ice with stirring and the remaining residues were partitioned between a minimum of 2-methyltetrahydrofuran and water (1:1 v/v). Once completely melted, the resulting solution was extracted twice with 2-methyltetrahydrofuran. The combined organic phase was dried over sodium sulfate, filtered and dried under vacuum. The resulting crude solid (85 % purity) was suspended in 10 mL of tert-butylmethylether, sonicated for 3 minutes and stirred vigorously (500 rpm) for 5 minutes. The solid was filtered, washed with a minimum of tert-butylmethylether (2 mL) and dried under vacuum. The desired product 7-bromo-3-(2,5-dichloropyrimidin-4-yl)-1H-indole (**15**) was obtained as a brown amorphous solid (1.31 g, 3.82 mmol), 73 % yield, 99 % purity.

LCMS: M+H (*m/z*) = 342.1, 344.0, 345.9, R_T = 1.91 min (5 – 100 % MeCN / 10 mM AmF aq., 3 min)
^{1}H NMR (400 MHz, DMSO-d_6) δ 12.48 (s, 1H), 8.80 (d, J = 0.5 Hz, 1H), 8.62 (d, J = 3.3 Hz, 1H), 8.49 (d, J = 8.0 Hz, 1H), 7.51 (dd, J = 7.7, 0.9 Hz, 1H), 7.29 – 7.09 (m, 1H).

Step 2:

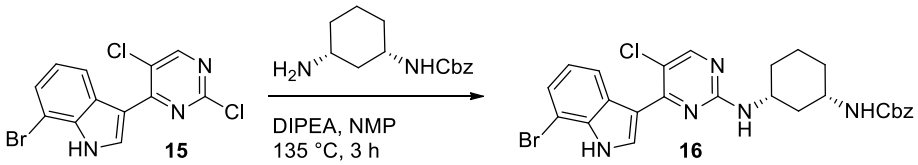

benzyl ((1S,3R)-3-((4-(7-bromo-1H-indol-3-yl)-5-chloropyrimidin-2-yl)amino)cyclohexyl)carbamate (16): To a suspension of 7-bromo-3-(2,5-dichloropyrimidin-4-yl)-1H-indole (**15**) (1.31 g, 3.82 mmol) in NMP (4.75 mL) was added benzyl ((1S,3R)-3-aminocyclohexyl)carbamate (1.42 g, 5.73 mmol) and diisopropylethylamine (2.00 mL, 11.46 mmol). The resulting mixture was heated to 135 °C for 4 hours using an oil bath. The reaction was then cooled down to room temperature and added dropwise to an aqueous HCl solution (12.0 mL conc. HCl /100 mL water). The resulting beige suspension was filtered and rinsed with water. The cake was then dried under vacuum, triturated in 50 mL of acetonitrile, filtered, dried again under vacuum. The desired product benzyl ((1S,3R)-3-((4-(6-bromo-1H-indol-3-yl)-5-chloropyrimidin-2-yl)amino)cyclohexyl)carbamate (**16**) was obtained as a yellow amorphous solid (1.75 g, 31.50 mmol), 83% yield, 98 % purity.

LCMS: M+H (*m/z*) = 555.7, R_T = 1.95 min (5 – 100 % MeCN / 10 mM AmF aq., 3 min)

Step 3:

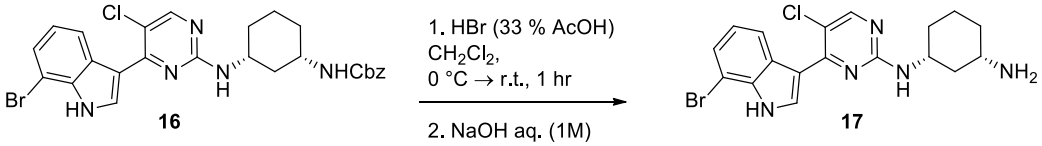

(1R,3S)-N1-(4-(7-bromo-1H-indol-3-yl)-5-chloropyrimidin-2-yl)cyclohexane-1,3-amine (17): (1R,3S)-N1-(4-(7-bromo-1H-indol-3-yl)-5-chloropyrimidin-2-yl)cyclohexane-1,3-amine ammonium bromide: To a suspension of benzyl ((1S,3R)-3-((4-(7-bromo-1H-indol-3-yl)-5-chloropyrimidin-2-yl)amino)cyclohexyl)carbamate **16** (1.75 g, 3.15 mmol) in dichloromethane (20 mL) in an ice bath. The mixture was then treated with HBr solution (5.0 mL, 33 % in AcOH). The mixture was allowed to warm to room temperature and left to stir for 2 hours. The mixture was then added portion-wise to *tert*-

butylmethylether (200 mL) and left to stir for 2 hours. The precipitate was filtered, washed with *tert*-butylmethylether, and dried under vacuum. The desired product (1R,3S)-N1-(4-(7-bromo-1H-indol-3-yl)-5-chloropyrimidin-2-yl)cyclohexane-1,3-amine ammonium bromide was obtained as amorphous yellow solid (1.76 g, 3.45 mmol), 99 % purity. The solid was then suspended in 2-methyltetrahydrofuran and partitioned with NaOH aq (1M) in a separatory funnell. The aqueous phase was extracted twice with 2-methyltetrahydrofuran. The combined organic phase was dried over sodium sulfate, filtered and evaporated under vacuum. The desired product (1R,3S)-N1-(4-(7-bromo-1H-indol-3-yl)-5-chloropyrimidin-2-yl)cyclohexane-1,3-diamine (**17**) was obtained as a off-white amorphous solid (1.23 g, 2.92 mmol), 92 % yield. 98 % purity.

LCMS: M+H (*m/z*) = 421.9, R_T = 1.37 min (5 – 100 % MeCN / 10 mM AmF aq., 3 min)

Step 4:

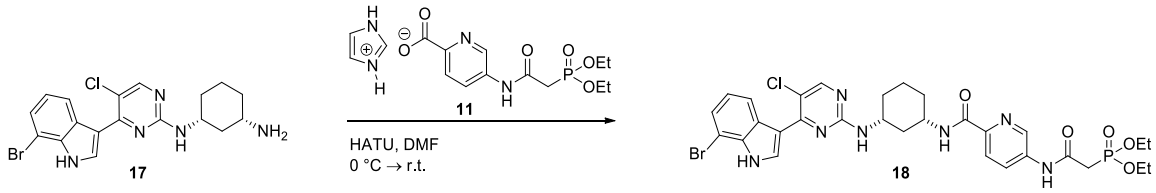

diethyl (2-((6-(((1S,3R)-3-((4-(7-bromo-1H-indol-3-yl)-5-chloropyrimidin-2-yl)amino)cyclohexyl)carbamoyl)pyridin-3-yl)amino)-2-oxoethyl)phosphonate (18): To a round bottom flask, 1H-imidazol-3-ium 5-(2-(diethoxyphosphoryl)acetamido)picolinate (**10**) (1.24 g, 3.22 mmol) was suspended in N,N-dimethylformamide (7.5 mL). To this solution DIPEA (1.02 mL, 5.85 mmol) was added and the solution was stirred until all was dissolved. The solution was then cooled to 0 °C and 1-[bis(dimethylamino)methylene]-1H-1,2,3-triazolo[4,5-b]pyridinium-3-oxid-hexafluorophosphate (HATU) (1.22 g, 1.22 mmol) was added. The reaction was stirred under nitrogen atmosphere for 5 minutes and turned bright yellow. Following this, (1R,3S)-N1-(4-(7-bromo-1H-indol-3-yl)-5-chloropyrimidin-2-yl)cyclohexane-1,3-amine (**17**) (1.23 g, 2.92 mmol) was dissolved in *N,N*-dimethylformamide (2.0 mL) and added to the solution. The reaction was stirred and left to slowly warmed up to room temperature. After 1h, the resulting mixture was then added dropwise to water (50 mL) and stirred vigorously (>800 rpm). Cold water (50 mL) was then added and the mixture was stirred for 2 hours. The resulting beige precipitate was then filtered, washed with water (100 mL) and dried under vacuum. The desired product (**18**) was obtained as a yellow amorphous solid (1.75 g, 2.43 mmol) 83 % yield, 97% purity.

LCMS: M+H (*m/z*) = 721.0, R_T = 1.68 min (5 – 100 % MeCN / 10 mM AmF aq., 3 min)

Step 5:

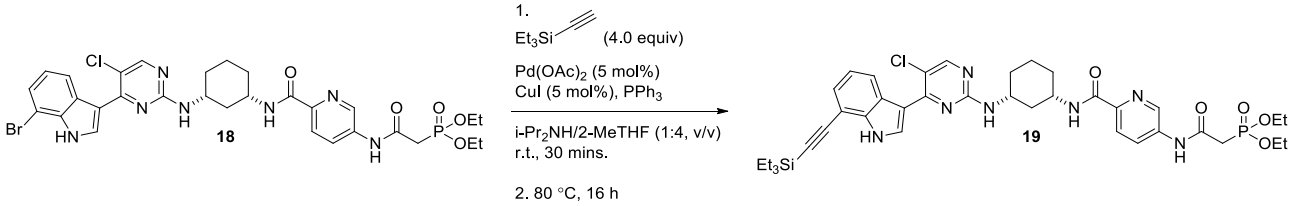

diethyl (2-((6-(((1S,3R)-3-((5-chloro-4-(7-((triethylsilyl)ethynyl)-1H-indol-3-yl)pyrimidin-2-yl)amino)cyclohexyl)carbamoyl)pyridin-3-yl)amino)-2-oxoethyl)phosphonate (19): To a solution of diethyl (2-((6-(((1S,3R)-3-((4-(7-bromo-1H-indol-3-yl)-5-chloropyrimidin-2-yl)amino)cyclohexyl)carbamoyl)pyridin-3-yl)amino)-2-oxoethyl)phosphonate **18** (500 mg , 0.695 mmol) in iPr_2NH / THF (1.39 mL, 1:4 v/v) under an nitrogen atmosphere were added catalytic amounts of CuI

(2.7 mg, 5 mol%), $Pd(OAc)_2$ (7.8 mg, 5 mol%), and triphenylphosphine (45.6 mg, 25 mol%). The solution was stirred for 30 minutes at room temperature, and then triethylsilylethyne (390 mg, 2.78 mmol) was added under vigorous stirring. The reaction mixture was then heated to 80 °C overnight. After being cooled to room temperature, the mixture was filtered, washed with methanol and concentrated under vacuum. The crude mixture was purified by normal phase column chromatography using 0 – 10 % MeOH / dichloromethane as eluent. The product was obtained as a light brown foam (340 mg) containing 8% of starting material. This foam was purified by reverse phase column chromatography (60 g) using 30 – 100 % MeCN / 10 mM AmF aq. Pure fractions were combined, frozen and lyophilized over 2 days. The desired product (**19**) was obtained off-white amorphous solide (320 mg, 0.41 mmol), 99 % purity, 59 % isolated yield.

LCMS M+H (*m/z*) = 777.9, R_T = 2.24 min (5 – 100 % MeCN / 10 mM AmF aq., 3 min)

Step 6:

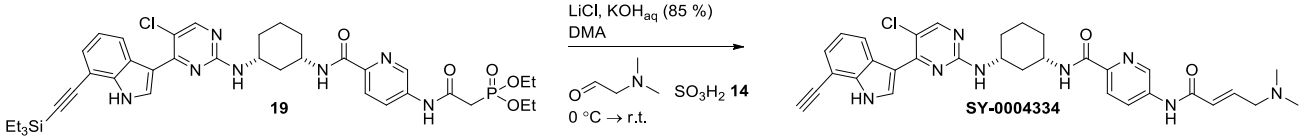

N-((1S,3R)-3-((5-chloro-4-(7-ethynyl-1H-indol-3-yl)pyrimidin-2-yl)amino)cyclohexyl)-5-((E)-4-(dimethylamino)but-2-enamido)picolinamide (SY-4334): To a 10 mL round bottom flask, diethyl (2-((6-(((1S,3R)-3-((5-chloro-4-(7-((triethylsilyl)ethynyl)-1H-indol-3-yl)pyrimidin-2-yl)amino)cyclohexyl)carbamoyl)pyridin-3-yl)amino)-2-oxoethyl)phosphonate **19** (320 mg, 0.410 mmol) was dissolved *N*,*N*-dimethylacetamide (4.1 mL). The reaction was stirred under nitrogen atmosphere. To this solution was added lithium chloride monohydrate (19.1 mg, 0.451 mmol) and the solution was stirred until dissolved. To the solution, 85 % KOH in water (1.15 mL, 41.0 mmol) was added and the reaction was left to stir at room temperature. After 15 minutes, 2.3 mL of *N*,*N*-dimethylaminoacetaldehyde solution in water (0.173 g, 1.02 mmol, 0.52 M) was added dropwise. The reaction was then left to warm to room temperature and was monitored by LCMS until judged complete. The crude solution was then added dropwise to 25 mL of water under vigorous stirring (>500 rpm), filtered, washed with water and dried under vacuum. The crude mixture was then purified via reverse phase column chromatography (25 g) using 10 – 60 % MeCN / 10 mM AmF. The pure fractions were then combined, frozen and lyophilized over two days. The desired product (**SY-4334**) was obtained as an off-white amorphous solid (95 mg, 0.159 mmol), 99 % purity, 39 % isolated yield.

LCMS M+H (*m/z*) = 597.0, R_T = 1.50 min (5 – 100 % MeCN / 10 mM AMF aq., 3 min.)
^{1}H NMR (400 MHz, DMSO-d_6) δ 12.04 (s, 1H), 10.54 (s, 1H), 8.86 (d, J = 2.3 Hz, 1H), 8.81 – 8.57 (m, 1H), 8.52 (d, J = 8.6 Hz, 1H), 8.37 (s, 1H), 8.30 – 8.16 (m, 2H), 7.98 (d, J = 8.6 Hz, 1H), 7.36 (t, J = 7.3 Hz, 2H), 7.31 – 7.08 (m, 1H), 6.78 (dt, J = 15.4, 5.7 Hz, 1H), 6.27 (d, J = 15.4 Hz, 1H), 4.55 (s, 1H), 4.08 – 3.71 (m, 2H), 3.05 (d, J = 5.6 Hz, 2H), 2.15 (s, 6H), 2.02 – 1.72 (m, 3H), 1.62 – 1.11 (m, 4H).